

Hydrothermal carbonization of industrial kraft lignin: Assessment of operational parameters

Salcedo-Puerto Orlando, Mendoza-Martinez Clara, Saari Jussi, Vakkilainen Esa

This is a Publisher's version of a publication
published by Elsevier
in Fuel

DOI: 10.1016/j.fuel.2024.132389

Copyright of the original publication:

© 2024 The Authors. Published by Elsevier Ltd.

Please cite the publication as follows:

Salcedo-Puerto, O., Mendoza-Martinez, C., Saari, J., Vakkilainen, E. (2024). Hydrothermal carbonization of industrial kraft lignin: Assessment of operational parameters. *Fuel*, 373, 132389. DOI: 10.1016/j.fuel.2024.132389

**This is a parallel published version of an original publication.
This version can differ from the original published article.**



Full Length Article

Hydrothermal carbonization of industrial kraft lignin: Assessment of operational parameters

Orlando Salcedo-Puerto^{*}, Clara Mendoza-Martinez, Jussi Saari, Esa Vakkilainen

School of Energy Systems, Lappeenranta-Lahti University of Technology LUT, Yliopistonkatu 34, FI-53850 Lappeenranta, Finland

ARTICLE INFO

Keywords:

Hydrothermal carbonization
Hydrochar
Industrial integration
Lignin

ABSTRACT

Lignin, one of the main constituents in wood and the second most abundant natural polymer, has generated great interest as a source for generating bio-based materials and fuels. The properties of lignin can be affected by various methods, for example, hydrothermal carbonization (HTC). The thermal treatment could thus be used to produce more suitable raw materials for added-value products. This work studies the relationship between the properties of the solid product (hydrochar) from HTC treatment and the choice of reaction conditions for typical HTC parameters: temperature – 200, 220, and 240 °C; residence time – 3, 6, 12, and 24 h; and water recirculation – 40, 60 and 80 vol% of process water (PW). The chemical composition of the hydrochar (HC) generated from industrial kraft lignin is evaluated along with their thermal degradation behavior under inert and oxidizing conditions by thermogravimetry. Compositional variations led to changes in characteristics such as volatile, fixed carbon, and ash content, varying to a greater or lesser extent according to the operational parameters. Although an increase in the temperature of the process leads to an increase in the calorific value of the hydrochar, this temperature change also leads to a slight decrease in the thermal stability of HC in oxidizing atmospheres. Additionally, the integration of a lignin HTC treatment process in a large modern Nordic pulp mill is presented, indicating minor disturbances when adding an HTC unit to the plant.

1. Introduction

Lignin is the world's second most abundant organic polymer after cellulose [1]. The primary industrial sources are side streams of pulp and paper mills and second-generation ethanol facilities [2]. Approximately 50 million metric tons of lignin per year are generated in the pulp mills [3], and the major portion is burned to energy on-site as a low-grade fuel, black liquor [4]. The most common source of commercially used lignin is kraft pulping, corresponding to approximately 85 % (approximately 100 million dry tons) of lignin recovered worldwide [5], and it is projected to reach 225 million tons by 2030 [6]. The growing interest in decarbonizing industrial processes has increased the interest in developing value-added products derived from lignin. The superior thermal stability and higher heating value of lignin compared to cellulose and hemicellulose indicate that lignin is a promising precursor for biochar production.

Lignin is composed of various linkages of three basic monolignol subunits, synapse alcohol, coniferyl alcohol, and p-coumaric alcohol, which become syringyl (S), guaiacol (G), and p-hydroxyphenyl (H)

groups [7]. The properties of lignin derived from the forestry industry depend on the raw material from which it is extracted and the pulp mill's production and separation processes. The concentration of the subunits varies depending on the biomass, i.e., softwood with 16–25 %-dry lignin in its composition has mainly G units, and hardwood with 23–35 %-dry lignin has mostly G and S units [8]. However, lignin is closely intertwined with cellulose and hemicellulose within plant fibers, making it difficult to degrade, dissolve, and use directly. Thus, industrial production yields a large amount of lignin residue, comprising enzymatic hydrolysis lignin, liginosulfonate, alkali lignin, and hydrolysis lignin, each stemming from various production processes [9]. Several studies have considered lignin as a renewable carbon source for chemicals and as a viable substitute for many fossil fuel-derived materials [10,11]. Recently, lignin has been used as a base in the structure of nanomaterials [12,13] and catalysts [14,15], as a feedstock for aromatic compounds and resins [16–18], and in the manufacture of bio-based electrodes for energy storage applications [19–21].

Hydrothermal carbonization (HTC) is a conversion process that has attracted attention for upgrading diverse wet organic streams into a

^{*} Corresponding author.

E-mail address: orlando.salcedo.puerto@lut.fi (O. Salcedo-Puerto).

<https://doi.org/10.1016/j.fuel.2024.132389>

Received 8 February 2024; Received in revised form 19 June 2024; Accepted 28 June 2024

Available online 2 July 2024

0016-2361/© 2024 The Authors. Published by Elsevier Ltd. This is an open access article under the CC BY license (<http://creativecommons.org/licenses/by/4.0/>).

homogeneous carbon-rich material (hydrochar), aqueous compounds, and gaseous streams (mainly CO₂). The HTC process occurs in an aqueous environment at moderate temperatures (180–280 °C) under autogenous pressure (up to 6.4 MPa) [22]. Based on the feedstock, the reaction times can vary from a few hours to several days [23,24]. HTC generally reduces the hydrogen (H) and oxygen (O) content of the feedstock through the removal of –OH groups, thus transforming organic mass into a high-energy-dense solid [25]. The solid yield ranges between 35 % and 85 % of the initial dry feedstock and has a higher heating value (HHV) of around 13–30 MJ/kg, depending on the initial energy content [24]. The main conversion mechanisms are dehydration and decarboxylation, which increase the final product's carbon content and energy value [25–27]. Process temperature, residence time, and ratio between feedstock and water are reported to be the main factors determining the decomposition rate [28]. The HTC process can be utilized with a wide range of raw materials irrespective of origin: agricultural and woody residues [29], municipal solid waste [30], food waste [31–36], and sludges [37–40]. The hydrochar produced can be used not only as a fuel but also in products and applications such as soil fertilizers, catalysts, energy storage, and adsorbents [41,42].

Recent studies have underlined the increased interest in HTC implementation for lignin upgrading. Kim et al. [43] reported significant improvement in lignin properties by HTC at temperatures of 150–280 °C, with a maximum increase in HHV of 23 %. Wikberg et al. [44] analyzed structural changes in kraft lignin during HTC, also in the presence of catalysts. HTC treatment at 240 °C for 22 h using an H₂SO₄ aqueous solution resulted in high carbon recovery (64 %) and a notable reduction of O and H, thus turning lignin into a hydrochar comparable to brown coal. Sangchoom and Monkaya [45] evaluated the absorption capacities of activated carbons produced from hydrothermally carbonized lignin at temperatures between 250–375 °C, similar to temperatures used in hydrothermal liquefaction [46]. Mao et al. [46] reported the effectiveness of HTC in combination with KOH as an activator agent in preparing carbon spheres from lignin. The best pore distribution and high sphericity were obtained at operational conditions of 270 °C and 7 h.

In addition to the operating parameters previously mentioned, the study of the recirculation of process water (PW) is a parameter whose interest has also increased. The recirculation of process water allows the reuse of water, minimizing the amount of freshwater needed for the process. The process water derived from the HTC process contains a variety of dissolved organic components, such as fatty and carboxylic acids, which can be recovered through separation or converted into gaseous fuels such as CH₄ and H₂ through catalytic and hydrothermal gasification [47,48]. Moreover, PW recirculation can potentially increase biocrude and hydrochar yields and decrease the cost of hydrothermal wastewater disposal, which could account for up to 90 % of waste treatment for the hydrothermal process [49].

Various studies have explored hydrothermal treatment of lignin for purposes such as wet oxidation to yield aromatic aldehydes, liquefaction for oil production, or hydrothermal gasification for methane generation. However, research specifically on hydrothermal carbonization of kraft lignin for hydrochar production remains scarce. In this study, we performed hydrothermal carbonization (HTC) of kraft lignin derived from an industrial pulp mill, under different HTC conditions, including residence time, temperature, and process water recirculation. In addition, an industrial integration simulation of the HTC process of lignin in a kraft pulp mill was carried out. To the best of our knowledge, the results presented in this study represent the first attempt to assess the effect that PW water recirculation has on the HTC of kraft lignin as well as the first attempt to evaluate the integration of this process in a pulp mill.

Thus, this research aims to evaluate the influence of these operational conditions would have in the physicochemical characteristics, energy properties, structure modification and thermal degradation profile of the hydrochar. Moreover, the simulation allows for a global, initial and brief evaluation of how the integration of a hydrothermal

carbonization process would impact the energy balance of a pulp mill. The operating parameters of the HTC unit in the simulation are selected from the parameters used in the experimentation phase and the characterization results of the hydrochar. Therefore, this study provides a better understanding of the nature of HTC treatment for a valuable resource like lignin and provides an approach to its large-scale implementation.

2. Materials and methods

2.1. Materials

The lignin used in this study was dried (8 wt% moisture) industrial softwood kraft lignin (IKL) from UPM Kaukas pulp and paper mill located in Lappeenranta, Finland. The sampling period of the lignin represented the normal process operating conditions of the mill. After sampling, the material was dried overnight in an oven at 105 ± 2 °C and stored in sealed polyethylene bags to minimize biological and chemical changes that can occur between the time of collection and the experimental procedures.

2.2. Experimental procedure

The applied methodology aims to simulate the one used in the HTC pilot plants [50,51] to work under operating conditions that help improve the scalability of the process. The experimental procedure is depicted in Fig. 1. The HTC tests were done in a closed stainless steel tube reactor (1 L inner volume and dimensions of 705 mm height and 42 mm inner diameter), and it had a flange connection at the top and a screw cap at the bottom. Two type K thermocouples monitored the internal temperature (245 mm and 645 mm from the top, respectively), while an additional thermocouple monitored the reactor's outer surface temperature. The reactor chamber was purged by flowing nitrogen gas. The increase in pressure inside the reactor was mainly caused by the generation of saturated water vapor and CO₂, without injection of additional gas (autogenous pressure). The pressure was measured with a pressure sensor (WIKA, model A-10, 0...40 bar gauge) with an accuracy of ≤ ± 0.5 %. The reactor was heated by a controllable electric resistance heating jacket and protected by a thick insulation layer and an outer steel sheet. The temperature level inside the reactor was maintained with a PID controller by varying the heat supply. Data from the temperature and pressure sensors were recorded automatically every 3 s. For each test, 25 g of IKL was mixed with 225 mL of water (1:9 ratio dry matter to water). Operating conditions are shown in Table 1.

Lignin-derived hydrochar was collected and separated from HTC liquor using a vacuum flask and a Büchner funnel with Whatman glass microfibre filter paper (grade GF/A) and subsequently dried in an oven at 105 ± 2 °C. Albeit analysis of HTC liquor is outside the scope of this paper, it is estimated to contain a variety of aromatic compounds (e.g., aromatic monomers, dimers, and low-molecular-weight oligomers) [52]. The presence of these compounds to a greater or lesser extent in the HTC liquor depends on factors such as temperature, time, solvents, catalysts, as well as the type of lignin used since its structure can vary based on its origin and the technique used for its extraction [53].

In this paper, the sample code IKL stands for original industrial kraft lignin. HTC-x-y and HTC-z stands for HC samples, where x, y, and z refer to process temperature, time, and recirculation ratio, respectively. The sample HTC-240-6 was selected for recirculation tests due to having the highest energy yield. For the recirculation test, only one recirculation was conducted. Remaining liquid from HTC-240-6, was used to prepare solutions with concentrations of 40 %, 60 %, and 80 % process water by volume. For instance, in the case of the 40 vol% of process water was used, and to complete the required 225 mL of liquid for the experiment, an additional 135 mL of pure water was added.

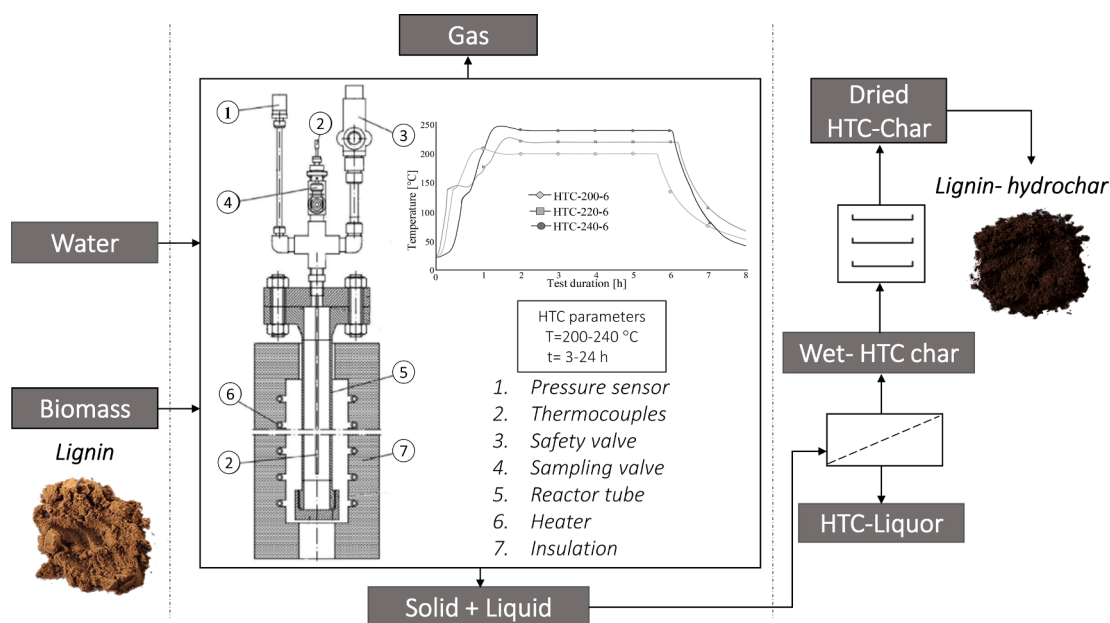


Fig. 1. HTC experimental unit and procedure.

Table 1
HTC operational parameters.

| Variable | Unit | HTC process settings | | | | | | | | | |
|---------------------|--------|----------------------|-----|-----|---|---|-----|----|----|----|----|
| Temperature | [°C] | 200 | 220 | 240 | | | | | | | |
| Time | [h] | | 6 | | 3 | 6 | 12 | 24 | | | |
| Mass ratio | – | | 1:9 | | | | 1:9 | | | | |
| Recirculation ratio | [vol%] | | 0 | | | | 0 | | 40 | 60 | 80 |

2.3. Analytical methods

2.3.1. Proximate, ultimate, and heating value analysis

The analyses were carried out in duplicate, and a mean value was reported. Moisture (MC), Volatile (VM), and ash (AC) contents were determined as mass percentages by proximate chemical analysis according to procedures of EN 18134 [54], EN 15148.18 [55], and EN 14775 [56] standards, respectively. Fixed carbon was calculated by subtracting the sum of VM and AC from 100 %. The HHV was measured with a Parr 6400 bomb calorimeter according to EN 14918 [57]. Ultimate analysis was performed using a TruSpec Micro-LECO CHN628 Series Elemental Determinator coupled with a 628S Sulphur Add-On Module according to the ISO 16948 [58] and ISO 16994 [59] standard procedures. The oxygen content was approximated as the difference between 100 % and the weight percentages of the major elements on a dry basis. The analyses were carried out in duplicate.

To assess the HTC process, the mass yield (MY), energy yield (EY), energy density factor (EDF), and fuel ratio (FR) were calculated with the following equations:

$$MY = \frac{m_{HC}}{m_{IKL}} \cdot 100\% \quad (1)$$

$$EDF = \frac{HHV_{HC}}{HHV_{IKL}} \quad (2)$$

$$EY = MY \cdot EDF \quad (3)$$

$$FR = \frac{FC}{VM} \quad (4)$$

Where: m_{HC} – HC mass (d.b.) [g], m_{IKL} – mass of IKL (d.b.) [g], HHV_{HC} – higher heating value of HC [MJ/kg] (d.b.), and HHV_{IKL} – higher heating

value of IKL [MJ/kg] (d.b.).

2.3.2. FTIR spectroscopy

To identify the chemical functional groups in the IKL and the HC, Fourier-transform infrared spectroscopy (FTIR) was performed with a Frontier MIR/FIR spectrometer (PerkinElmer Inc.) coupled with a universal diamond crystal ATR module in the range of 400–4000 cm^{-1} with a resolution of 4 cm^{-1} . Detailed information can be found in [Supplementary Material A](#).

2.3.3. Thermogravimetric analysis and mass spectrometry (TGA-MS)

Thermogravimetric analysis coupling with mass spectrometry (TGA-MS) was performed with an STA 449C thermogravimetric analyzer (Netzsch Instruments, Germany). For each test, about 10 mg of the sample was placed inside an Al_2O_3 sample holder, the furnace was sealed, and high purity (99.9995 %) nitrogen was used to purge the air. The sample was heated at a rate of 5, 10, and 20 $^\circ\text{C}/\text{min}$ from room temperature to 900 $^\circ\text{C}$. Two different gas atmospheres were used: high-purity nitrogen for pyrolysis conditions (inert atmosphere) and compressed air for combustion (oxidizing atmosphere). A constant gas flow rate of 250 ml/min was set in both cases.

The released gas species were analyzed with a QMS 403 Aeolos Quadro Mass Spectrometer to obtain the evolution curves. The mass spectra data was calibrated by conversion of the raw time of flight data to molecular weight to get the standard peaks in the spectrum. The main lignin and hydrochars MS peaks are identified based on literature data. The chemical noise background in the spectrum was isolated through baseline subtraction. A normalization method using the total ion current was applied to eliminate any systematic effects of sample degradation and variation in the detector sensitivity.

2.4. Kinetic analysis

The *iso*-conventional kinetics models Flynn-Wall-Ozawa (FWO) [60,61], Kissinger-Akahira-Sunose (KAS) [62,63], and Friedman [64] methods were used. The kinetic parameters of the samples were calculated assuming the devolatilization phenomena as a single reaction. The models are based on the Arrhenius equations to determine the pre-exponential factor (A) and activation energy (E_a) and to predict possible thermal decomposition mechanisms of the lignin-based hydrochars. Detailed information can be found in [Supplementary Material A](#).

2.5. Lignin HTC- industrial integration simulation

The energetic impact of implementing a lignin HTC treatment process on a large modern Nordic pulp mill was evaluated with IPSEpro steady-state equation-based process simulation software. The kraft pulp mill and recovery boiler are the same as those presented in [65]. The lignin removal and HTC treatment are considered as retrofits to the existing mill and recovery boiler. The component models of the boiler, steam cycle, and HTC system are primarily based on those presented originally in the mill, its recovery boiler, and steam cycle are listed in [Table 2](#).

The considered mill produces 1.6 million air-dried tons (ADt) of bleached kraft pulp annually during 8400 h of operation. 1.5 metric tons of black liquor dry solids (composition assumed the same as in [65]) are produced per ADt of pulp; the fraction of lignin in the black liquor dry solids is estimated at approximately 31 %. The main effect of lignin removal will be the reduction of boiler fuel input, resulting in a reduction of steam generation and flue gas flow rate [66].

The lignin removal rate was set at 7.5 t/h of dry lignin. Amounting to less than 10 % of total lignin, it was assumed that this amount could be separated relatively easily without adversely affecting the quality and homogeneity of the separated lignin or excessively reducing the boiler steam production [66,67] or turbine extraction pressure levels. The lignin removal power consumption was estimated at 80 kWh/t [68].

The final product, whether raw lignin or the lignin hydrochar, is first dewatered to a wet mass basis moisture content of MC = 30 % in a belt press and then thermally dried to final product moisture of MC = 10 %. A specific power consumption of 20 kWh_{el}/t_d is assumed for the dewatering press [69]; the thermal drier is assumed to have specific consumptions of 1.2 kWh_h/kg_{evapH2O} and 200 kWh_{el}/(kg/s)_d of heat and power, respectively [65].

2.6. Statistical methods

The level of variance within groups of samples for proximate, ultimate, and heating value properties was evaluated with MATLAB 2020a software package. The statistical significance ($\alpha = 0.05$) between the samples was evaluated with one-way analysis of variance (ANOVA) and

Table 2
Main operating parameters of the considered pulp mill.

| | Parameter | Value |
|-------------------|---|---------------------|
| Production | Operating hours [h/a] | 8400 |
| | Pulp production [t _{AD} /a] | 1.6·10 ⁶ |
| Energy | Steam use, pulp mill [t/h] | 775 |
| | Power use, pulp mill [kWh/t _{AD}] | 552 |
| | Gross power generation [MW _{el, gen}] | 213.7 |
| | Net power sold [MW _{el, net}] | 146.1 |
| Boiler | Dry solids to boiler [t _{ds} /d] | 7611 |
| | Dry solids x _{ds} , firing liquor [-] | 0.83 |
| | Main steam production [t/h] | 1201 |
| | Main steam temperature [°C] | 510 |

multiple post hoc t-tests using the Bonferroni correction to adjust the significance level and consider the statistically significant results of all pairwise comparisons. Moreover, a paired-sample t-test was developed to compare the significant difference between two selected HC samples for the same measured variable; statistical results are reported in [Supplementary Material B](#).

3. Results and discussion

3.1. Proximate and ultimate analyses

Proximate and elemental analysis results are shown in [Table 3](#). IKL had a rather low ash content (AC) of only 1.17 wt%, which decreased significantly (75 %) after HTC due to the dissolution of ash-forming compounds in the aqueous phase. Low AC reduces the incidence of problems such as agglomeration, fouling, and corrosion, thus facilitating boiler and combustor design [70,71].

Devolatilization and depolymerization reactions during HTC generally result in loss of volatiles [29]. In this study, the volatile matter (VM) decreased as temperature increased. HTC-240-6 sample reported a maximum reduction of 10.8 % from IKL. Regarding the reaction time, a maximum VM reduction of 13.2 % was obtained for HTC-240-12 (61.6 wt%) compared to IKL. However, with an increase in the reaction time, the VM increased to 67.3 wt% at 24 h, indicating the possible re-absorption of degradation products from the aqueous phase due to prolonged reaction times; a similar effect was observed when the water phase in the reaction has a high content of dissolved components [72,73]. The fixed carbon (FC) showed a slight increase with higher temperatures and longer reaction times. The maximum value for FC was found for the sample HTC-240-12 (38.0 wt%). Similar results have been obtained in previously reported hydrothermal conversion tests of lignin [43]. For instance, Ischia et al. [74] highlighted that due to the recalcitrant nature of lignin, the proximate composition of the hydrochar slightly changed when the reaction temperature increased from 200 to 280 °C at 0 h, having a more significant degradation at longer residence time under the previous conditions. Kang et al. [75] reported more significant changes in the hydrochar composition at longer residence when moderate temperatures are used, having a 25 % VM reduction and 40 % FC increment at 225 °C and 20 h reaction time. When considering the recirculation tests, the change in VM was found to be negligible, as increased the amount of process water. This increase in VM can be attributed to the adsorption/desorption of components present in the recirculated PW. A similar effect has been reported by Cai et al. [76] Rodríguez et al. [77], and Li et al. [78].

Temperature and time were the main variables influencing the properties and composition of the hydrochar (HC), with a moderate influence of the PW recirculation. Significant reduction in AC and VM was observed between the hydrothermally treated samples and the IKL. The statistical analysis with one-way ANOVA (significance level of 0.05) showed that the behavior observed for HTC-40 % regarding AC was significantly different in HC samples treated at 240 °C [F(4,19) = 6.67, p < 0.005]. Probably, a higher content of hydrophilic compounds from the liquor was adsorbed in the HC during HTC treatment at 40 % recirculation. For HTC-60 % and HTC-80 %, no statistical difference was found between the treatments except for HTC-200-6 [F(7,31) = 1.93, p = 0.12]. As for VM, no significant difference was found between the group means of recirculation treatments and HTC-240-24 [F(3,15) = 4.2, p = 0.03]. However, for the other treated samples, including untreated lignin, a significant difference in VM was observed [F(5,23) = 18.6, p < 0.005]. The fuel ratio (FR) of kraft lignin (0.39) was improved after the hydrothermal process. The FR increased from 0.51 to 0.58 as process temperature increased from 200 to 240 °C and 0.56 to 0.62 as the residence time increased from 3 to 12 h, respectively. As mentioned above, VM increased when residence time exceeded 12 h. Consequently, the FR decreased from 0.62 to 0.42 between 12 and 24 h of residence. Additionally, the FR of the samples when process water recirculation

Table 3
Proximate and elemental compositions of the samples.

| Properties | C | H | N | S | O* | AC | VM | FC | FR |
|----------------------------|-------------------------|------------------------|------------------------|------------------------|------------------------|------------------------|------------------------|------------------------|------------------------|
| Samples | (wt.%, db) | | | | | (wt.%, db) | | | |
| IKL | 63.97 _(0,10) | 6.14 _(0,04) | 0.17 _(0,01) | 2.17 _(0,01) | 26.4 _(0,01) | 1.17 _(0,02) | 70.9 _(0,93) | 27.9 _(0,94) | 0.39 _(0,02) |
| Temperatures | | | | | | | | | |
| HTC-200-6 | 65.7 _(0,07) | 5.98 _(0,02) | 0.16 _(0,02) | 2.34 _(0,02) | 25.3 _(0,03) | 0.53 _(0,02) | 65.8 _(0,33) | 33.7 _(0,39) | 0.51 _(0,00) |
| HTC-220-6 | 65.8 _(0,06) | 5.71 _(0,02) | 0.18 _(0,01) | 2.22 _(0,04) | 25.8 _(0,02) | 0.34 _(0,04) | 64.9 _(0,11) | 34.7 _(0,12) | 0.53 _(0,00) |
| HTC-240-6 | 65.9 _(0,08) | 5.22 _(0,02) | 0.20 _(0,00) | 2.17 _(0,01) | 26.1 _(0,05) | 0.32 _(0,08) | 63.3 _(0,17) | 36.4 _(0,12) | 0.58 _(0,00) |
| Time | | | | | | | | | |
| HTC-240-3 | 65.7 _(0,16) | 5.94 _(0,03) | 0.19 _(0,03) | 2.2 _(0,04) | 25.7 _(0,13) | 0.32 _(0,04) | 63.8 _(0,46) | 35.9 _(0,48) | 0.56 _(0,01) |
| HTC-240-6 | 65.9 _(0,08) | 5.22 _(0,02) | 0.20 _(0,00) | 2.17 _(0,01) | 26.1 _(0,05) | 0.32 _(0,08) | 63.3 _(0,17) | 36.4 _(0,12) | 0.58 _(0,00) |
| HTC-240-12 | 65.4 _(0,05) | 5.45 _(0,20) | 0.18 _(0,02) | 1.63 _(0,05) | 26.9 _(0,26) | 0.40 _(0,05) | 61.6 _(0,64) | 37.9 _(0,59) | 0.62 _(0,01) |
| HTC-240-24 | 65.7 _(0,22) | 5.61 _(0,03) | 0.20 _(0,03) | 1.66 _(0,01) | 26.6 _(0,22) | 0.30 _(0,02) | 67.3 _(0,71) | 32.4 _(0,70) | 0.48 _(0,01) |
| Recirculation ratio | | | | | | | | | |
| HTC-40 % | 63.8 _(0,77) | 5.53 _(0,18) | 0.17 _(0,05) | 1.71 _(0,07) | 28.4 _(0,84) | 0.45 _(0,01) | 68.0 _(0,11) | 31.5 _(0,09) | 0.46 _(0,00) |
| HTC-60 % | 63.6 _(0,58) | 5.62 _(0,06) | 0.20 _(0,01) | 1.69 _(0,00) | 28.5 _(0,59) | 0.35 _(0,03) | 67.9 _(0,21) | 31.8 _(0,24) | 0.47 _(0,00) |
| HTC-80 % | 64.3 _(0,03) | 5.69 _(0,02) | 0.19 _(0,01) | 1.64 _(0,03) | 27.9 _(0,05) | 0.36 _(0,05) | 67.3 _(0,25) | 32.4 _(0,30) | 0.48 _(0,01) |

* dry-ash free- basis. (...) Standard deviation.

was performed was significantly lower than those of the temperature and residence time tests. This reduction is attributed to the lower FC and higher volatile matter VM in the hydrochar when the recirculation of process water was carried out. When compared to lignocellulosic biomass, the fuel ratio of the material is expected to be much higher after hydrothermal treatment. This is because lignocellulosic biomass has a more heterogeneous composition, leading to greater degradation during the hydrothermal process [29].

In the samples analyzed, the elemental carbon content (C) increased slightly as the process severity intensified, reaching a maximum value of 66 wt%, reported by sample HTC-240-6. The low change in relative carbon content, along with the resulting high mass yield (section 3.2) is an indication of the mild reactivity of the IKL under the working temperatures. It should be noted that the method implemented for lignin extraction influences its final structure. Consequently, lignin obtained from different extraction processes has different chemical structure, functionalization, and physical and chemical properties [79], thus influencing its reactivity. There was a reduction in the hydrogen (H) and oxygen (O) content of the HC in relation to IKL. A slight increase in the oxygen content was observed among the hydrochar samples when modifying the operational parameters. This relative increase in the oxygen content as temperature rises can be due to the slight increase of carbon content and the simultaneous reduction of hydrogen. This compositional change could be derived from demethylation reactions. As noted earlier, the method of lignin extraction influences its structure and functional groups. Previous studies have indicated that kraft lignin has a high concentration of methoxy groups (OCH₃), as well as the presence of methyl (CH₃), and methylene (CH₂) groups in the aliphatic region of the phenylpropane units on which lignin is based [80]. It has been pointed out by Kim et al [43] that methoxy and methyl groups in lignin may be easily fractured during HTC. This fracture may lead to a slightly lower concentration of these groups in the hydrochar. The reduction of these groups can be appreciated in the FTIR spectrum (Supplementary material A). The spectrum shows a decrease in the bands at 2935 cm⁻¹ (CH₃ and CH₂ groups) and 1450 cm⁻¹ (OCH₃ groups) as the temperature increases. Similar reductions in these groups have been reported in previous experiences when thermally treating lignin, being this attributed to demethylation reactions [44].

On the other hand, this slight increase in oxygen content could also be attributed to generating reactive intermediates or free radicals within the process capable of initiating oxidation reactions [81]. These intermediates can react with the oxygen present in the system to form oxygen-containing functional groups on the lignin, increasing the

content of oxygen functional groups on the surface while increasing the operational time (mainly phenolic hydroxyl, lactonic and carboxyl groups), as indicated by [82]. The samples where recirculation was performed have greater exposure to these intermediates since these can be present to a greater extent, which could lead to higher oxidation of organic compounds in the hydrochar and a higher concentration of these oxygen functional groups on its surface.

The nitrogen (N) content showed a slight increase, whereas the sulfur (S) content remains practically unchanged, which aligns with previous studies [77,83,84]. Kraft lignin has an average sulfur content between 1.5 and 3 wt%. Sulfur can be found in lignin as sulfate ions, elemental sulfur, adsorbed sulfide, and organically bound sulfur [85]. High concentrations of N and S during combustion promote the generation of some pollutants such as nitrogen oxides (NO_x, mainly NO and NO₂), sulfur oxides (SO_x, mainly SO₂), as well as other sulfide-based pollutants such as carbonyl sulfide (COS) and hydrogen sulfide (H₂S) [86].

The van Krevelen's diagram in Fig. 2 shows the molar ratios of oxygen and hydrogen to carbon (O/C and H/C, respectively) for IKL and HC. Additionally, it includes the atomic ratios of various solid fuels, agricultural waste, and treated biomass available in different databases [87], allowing for a visual comparison of the samples with other solid fuels as their atomic ratios change. The diagram shows that the variation of the operational parameter influences the H/C and O/C ratios. The shift of the atomic to a lower left side indicates that dehydration and decarboxylation reactions are taking place. Previous experiences on hydrothermal treatment of lignocellulosic biomass have suggested that dehydration dominates over decarboxylation during the HTC processes [88]. This dehydration effect can be clearly seen by the reduction of the -OH band between 3500 and 3200 cm⁻¹ of the FTIR spectrum (Supplementary Material A). The same reduction of this band has been previously reported for lignin and different lignocellulosic biomass, being attributed to the same reaction mechanism [43,89]. Nevertheless, other minor mechanisms may occur under the hydrothermal carbonization of biomass such as demethylation [90]. It can be observed that as temperature and time increase, the H/C ratios decrease mainly as a product of the reduction of the hydrogen content of the hydrochar, following a demethylation line trend.

The H/C and O/C average values of the HC were 1.04 and 0.31 respectively. As previously mentioned, the recirculation test showed an increased VM content which may be attributed to the adsorption of species present in the PW, which would lead to the increase of the O/C ratios. A similar shift of the O/C ratios was reported by Wüst et al. [91] when hydrothermally treating brewer's spent grains. The authors

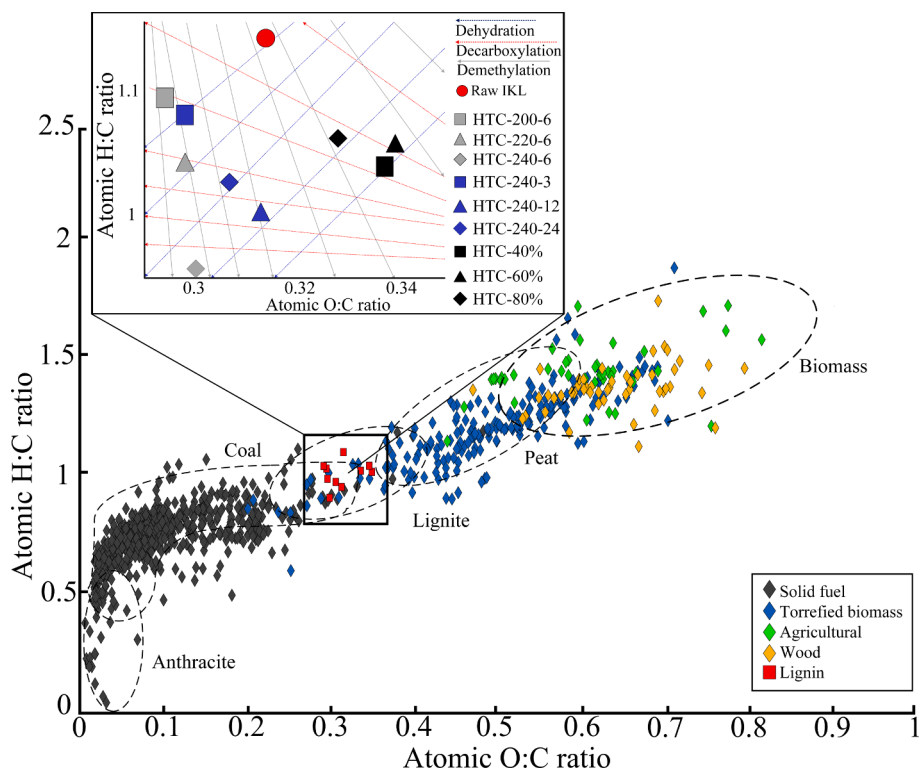


Fig. 2. van Krevelen's diagram of produced hydrochars and different solid fuels. Data points corresponding to biomass and biomass-derived solid fuel are sourced from Phyllis database [87].

attributed this behavior to the adsorption of carboxylic acids and aldehydes from the PW of the hydrochar surface. The atomic ratios of the lignin-derived HC are similar to those reported for lignite: O/C between 0.33 and 0.40 and H/C between 0.07 and 0.08 [92]. Similarly, the average C content in the HC samples is close to anthracite, whose values are between 62–79 wt% [92,93]. These characteristics in the content of C, H, and O make lignin-derived hydrochar have energy values similar to those of lignite coke and some bituminous coals [94]. The energy content is discussed in section 3.2.

3.2. Mass and energy yields

Mass and energy yields, HHV, and EDF values are shown in Fig. 3. High values of MY were obtained when compared to previously reported studies, such as MY of 61 % at 240 °C for 22 h [44] and 81.92 % at 220 °C for 30 min [43]. Nevertheless, when analyzing the TGA curve of the raw lignin in [44], lignin main degradation begins at temperatures close to 220 °C and has already lost approximately 17 wt% of its initial mass, indicating that laboratory-extracted lignin is more prone to be degraded at early temperatures compared with the industrial kraft lignin used in the present study. Section 3.3 shows that IKL starts its main degradation at around 250 °C. At this stage, the IKL has lost nearly 5 wt % of its initial mass, thus indicating greater resistance to degradation. On the other hand, [43] reported an ash content of 17.8 wt%, much higher than the IKL of the present study, 1.17 wt%. Due to the hydrophilic nature of the ash-forming components, the ash content in HC tends to decrease during the HTC process at temperatures below 240 °C [95–97]. Higher ash content and lower thermal stability explain why these previous studies had lower hydrochar mass yield. However, when compared with industrial lignin, the MY values are consistent. Musa et al. [97] reported MY of 88–90 % at 200–240 °C, where softwood-derived industrial kraft lignin is also used. High MY values indicate that the lignin does not undergo drastic degradation in this temperature range, being partially carbonized. Less than 12 wt% of the lignin was converted into liquid and gaseous products at temperatures below

240–250 °C. In the present work, the mass loss slightly increased with temperature and time, from 5 to 9 % and 7 to 14 %, respectively. No significant difference was observed between the group means for the 3 h and 6 h residence time treatments [$F(3,7) = 1.28, p = 0.3943$]. Additionally, Post hoc comparison using multiple t-tests indicated no statistically significant differences between HTC-240-12 (87.0 %±0,023) and HTC-240-24 (85.9 %±0,003). It should be noted that the solids yield for water-insoluble feedstocks, such as kraft lignin, is 100 % at the beginning of the HTC process, while it is 0 % for soluble feedstocks. For insoluble raw materials, this means that the solid recovered at the end of the hydrothermal process consists of both thermally converted and the original raw material that has not undergone thermal conversion [44]. The high mass yield of the process can be attributed to the high thermal stability of the kraft lignin and the minor fraction that dissolves in water at the selected operational temperatures.

In the case of recirculation test an opposite tendency was observed: the MY increased from 79 % for the HTC-40 % sample to 86 % for the HTC-80 % sample. Significant difference of HTC-40 % with all samples except HTC-60 % [$F(7,15) = 28.49, p < 0.005$] and significant difference of HTC-80 % with HTC-200-6, HTC-240-3 and HTC-40 % [$F(3,7) = 86.13, p < 0.005$], was observed. The increase in the HTC-40 % and HTC-80 % MY indicates that part of the organic compounds that were previously dissolved into the aqueous phase, e.g., phenolic derivatives, could successfully re-polymerize to the solid product. Similar results were obtained by Wang et al. [72] for the recirculation effects of PW on the solid products of the HTC of microalgae, who reported MY increase as the number of recirculations increased. Although only a single recirculation was carried out in this study, the PW concentration increased in relation to the pure water used in the HTC treatments. The increase in the concentration of the recirculated PW makes it possible to compare, to some extent, the results obtained when increasing the number of recirculations. In both cases, there is a tendency to have a greater amount of dissolved organic matter in PW, and this is the material that would be re-polymerized, thus increasing the mass yield.

The HHV of IKL (26.98 MJ/kg) slightly increased after the

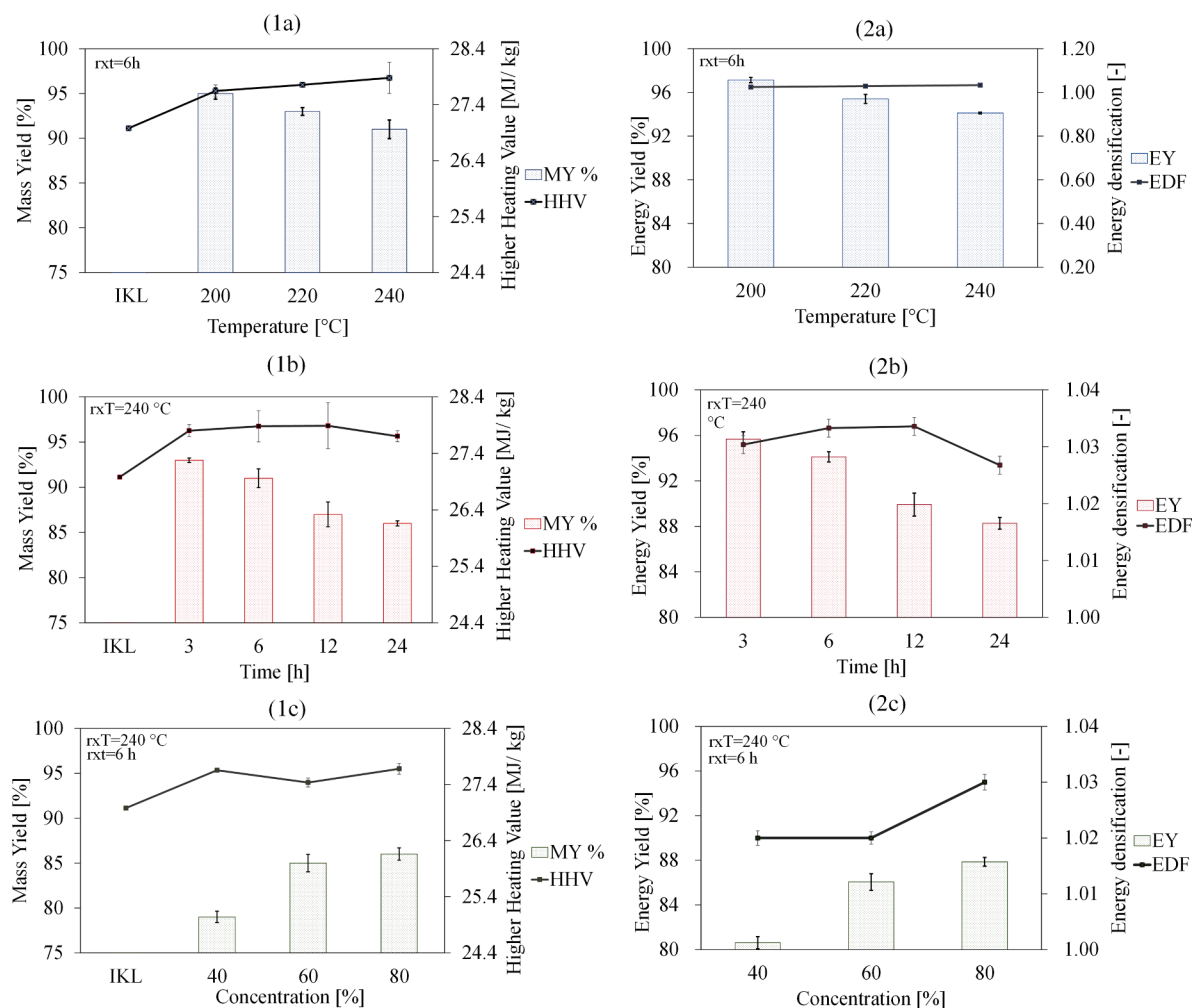


Fig. 3. MY, HHV, EY, and EDF of hydrochars as a function of (a) temperature, (b) time, and (c) recirculation.

hydrothermal treatments. The analysis of the variance showed a significant difference between IKL and hydrochar HHV [$F(9,39) = 13.3$, $p < 0.005$]. The increase in HHV is attributed to the higher C and lower O and H content. Although in the present study, the calorific value of the hydrochar was measured by a bomb calorimeter, there are empirical mathematical correlations that allow to better notice the correlation between the HHV and the elemental composition [98]. For instance, Ischia et al. [99] calculated the HHV of cellulose-derived hydrochar using Dulong's formula, highlighting that the increasing elemental carbon content of hydrochar is the main factor responsible for the enhancement of the HHV. The largest HHV increase was obtained for HTC-240-6 (27.89 MJ/kg). The increase of the reaction time does not lead to significant changes in HHV. Similar results have been reported by Gao et al. [100] when hydrothermally treating water hyacinth at 240 °C up to 24 h. The results showed a significant increase in the HHV up to 8 h residence time (20.63 MJ/kg). However, at longer reaction times, these caloric values fluctuate decreasing to 18.6 MJ/kg. As earlier mentioned, in hydrothermal processes, both temperature and time play crucial roles in determining the outcome, but temperature generally is the primary driver of the process [74]. Although longer reaction times enable more extensive transformations, insufficient temperature can restrict the formation of desired products. Nicolae et al. [101] have pointed out that higher temperatures enhance degradation reactions according to Arrhenius kinetics, thus, even with prolonged reaction times, the inadequate temperature may impede the desired chemical changes. Additionally, the composition of the feedstock also influences the process, as different biomasses are more or less prone to degradation. A significant

difference was found for recirculation samples HTC-40 % and HTC-60 % compared to the rest of the treated samples. The concentration of the components that make up lignin varies during thermal degradation, influencing the energy content of the final product. For instance, in the present work, the concentration of guaiacol (whose HHV is 28.91 MJ/kg) increased after HTC, while the concentrations of other products with lower HHV, such as vanillin, homovanillin, or coniferyl, decreased (see section 3.4). Any deposition of these compounds or their intermediates with lower HHV on the surface of the HC would decrease its overall heating value, which could be related to the decrease in HHV of HTC-240-24 and the increase in its VM content. No significant differences in HHV were found among the other time variation tests.

As a general trend, a decrease in MY and an increase in HHV result in energy densification of the sample during thermal degradation. For temperature and time variations, high values of EY were obtained, between 97.13 and 94.11 %, respectively. It is possible to appreciate from Fig. 3 that the EY decreased as temperature and time increased. The opposite trend was followed by the PW recirculation samples, which are in accordance with the data reported by Uddin et al. [102] and Arauzo et al. [103], where the EY values tended to increase as the number of recirculations increased, or as the concentration of dissolved components in the PW increased. The slight increase in HHV and MY in the recirculation tests indicated that, although the energy content of the samples was improved, these, in turn, had a lower loss in their net mass at the end of the HTC process.

3.3. Thermogravimetric analysis

The thermogravimetric (TG) and the corresponding derivative (DTG) curves of the degradation process of KL and HC at a heating rate of 20 °C/min were divided into three stages, as shown in Fig. 4. For both inert and oxidative atmospheres, the initial mass loss of about 1 % is attributed to the partial loss of lightweight volatiles and moisture evaporation. Table 4 shows the temperature values and the maximum mass loss rate for each reaction stage of the lignin-derived hydrochar in inert and oxidative atmospheres.

Under an inert atmosphere, after dehydration takes place, there is an accelerated increase in the mass loss rate. Stage I occurs at temperatures between 130–330 °C. The largest weight loss of stage I was approximately 14 wt% at temperature ranges of 200 and 330 °C, which can be attributed to the lignin glass transition and microscopic surface changes [104]. Above 200 °C, lignin softens, and its particles fuse, eliminating some lignin structural units, modifying its structure, and releasing a small amount of volatiles [83,105]. In stage I, DTG curves were asymmetric with a smooth shoulder after 260 °C, which changed to some extent based on the sample. Lofti et al. [106] attributed this shoulder to the cleavage of C–H groups between adjacent aromatic rings, resulting in the formation of some aromatic compounds. In this range of temperatures, the cleavage of α -ether bonds also takes place in some phenolic compounds, forming quinone methide resulting in the rupture of β -ether bonds at temperatures close to 250 °C, as indicated by Kawamoto [8]. The breaking of the C–H bonds and the ether bonds can

be appreciated from the results on Supplementary material A, where the FTIR curve showed a decrease in the density of the C–H group of the aromatic rings and ether groups in the hydrothermally-treated samples as the severity of the process increased.

Stage II (330–510 °C) reported the maximum weight loss rate of the HC and KL at temperatures near 400 °C. In stage II, the homolysis reactions of the lignin weakest bond, like β -O-4, produce phenethyl and phenoxy radicals [106]. Albeit during the hydrothermal process at temperatures between 200–240 °C some aromatic groups are detached from the lignin, its polymer matrix, and main structural composition have undergone only a mild breakdown, as the primary decomposition of the lignin backbone takes place at temperatures above this range [105]. This explains why the HC and raw IKL have similar behavior in the pyrolytic zone. Similar behavior was reported by Ischia et al. [74] for lignin-derived hydrochar produced at 220 and 250 °C, where there was no significant difference in the maximum weight loss rate between these two samples. Close to 300 °C, the TG curve drops significantly, indicating that a large amount of organic matter is degraded. Li et al. [107] indicated that in this stage, the side chain products crack, and the lignin monomer connecting network starts to break down, forming a mass of lignin monomers, and as a result of the secondary cracking of side chains, some unstable functional groups with some light gases are formed. Likewise, Wądrzyk et al. [108] stated that it is at temperatures above 300 °C where the primary decomposition of lignin begins, having a greater cleavage of the C–C and C–O bonds of the guaiacyl and syringyl units, giving rise to the formation of phenolic compounds such as

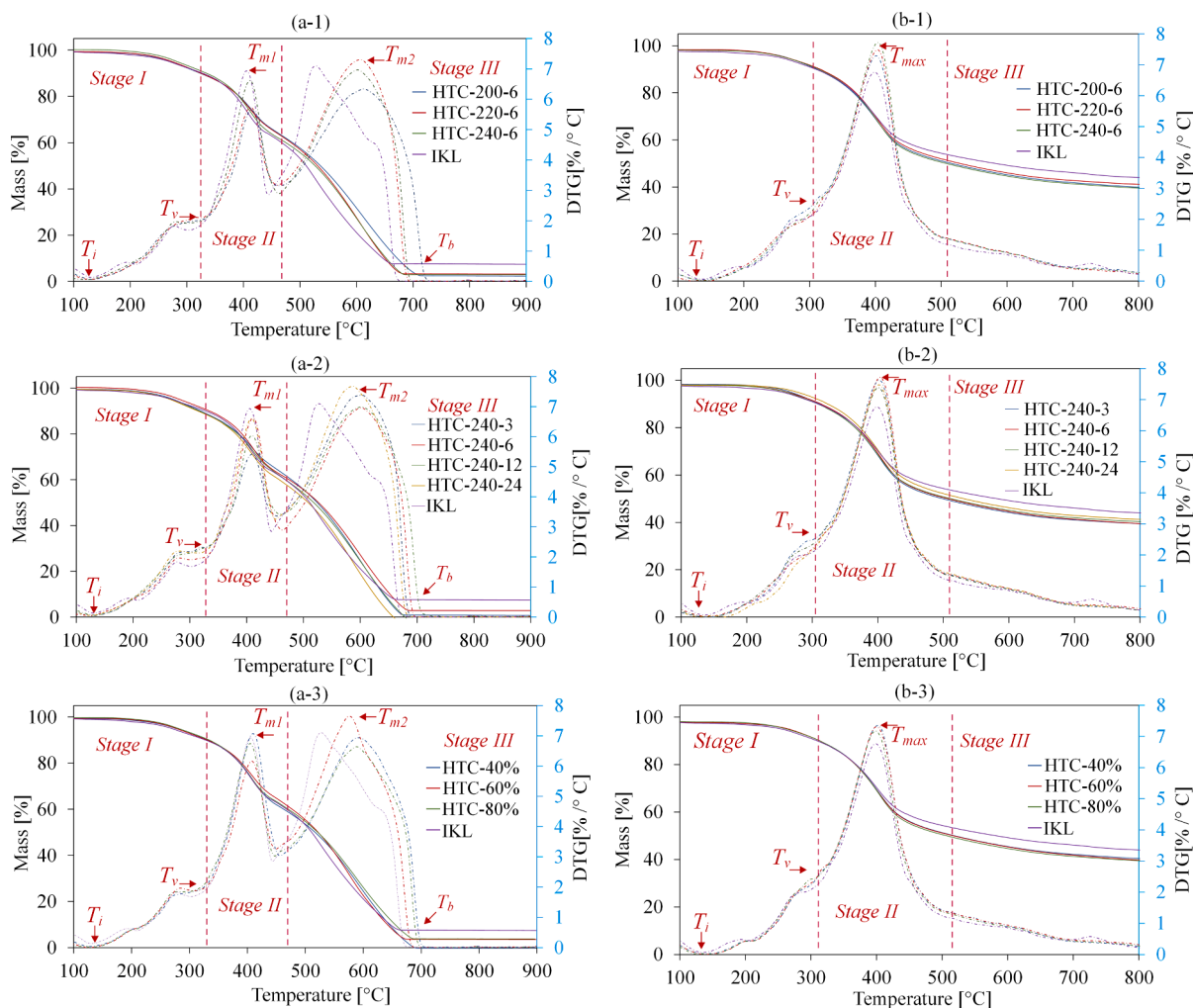


Fig. 4. TGA of IKL and produced hydrochar: (a) air atmosphere, (b) N2 atmosphere.

Table 4

The temperatures of each characteristic degradation stage and the maximum degradation rate at inert and oxidative atmospheres.

| Sample | Inert | | | | | | Oxidative | | | | | | |
|------------|-----------------|-----------------|---------------------|-----------------------|-----------------|-----------------------------|-----------------|-----------------|--------------------|-----------------------|--------------------|-----------------|-----------------------|
| | Stage I | | Stage II | | Stage III | | stage I | | stage II | | stage III | | |
| | T_i^a (°C) | T_f^b (°C) | T_{max}^c (°C) | DTG_{max} (%/°C) | T_h^d (°C) | Residue ^e (%) | T_i^a (°C) | T_f^b (°C) | T_{m1}^f (°C) | DTG_{max} (%/°C) | T_{m2}^g (°C) | T_b^h (°C) | DTG_{max} (%/°C) |
| IKL | 121 | 333 | 398 | 6.76 | 581 | 43.14 | 130 | 354 | 405 | 6.93 | 527 | 674 | 7.1 |
| HTC-200-6 | 134 | 333 | 401 | 7.29 | 514 | 38.84 | 131 | 351 | 414 | 5.65 | 612 | 714 | 6.34 |
| HTC-200-6 | 121 | 337 | 403 | 7.49 | 526 | 40.32 | 129 | 352 | 412 | 5.74 | 606 | 693 | 7.31 |
| HTC-240-6 | 138 | 335 | 403 | 7.72 | 508 | 38.45 | 122 | 358 | 411 | 6.62 | 601 | 687 | 6.97 |
| HTC-240-3 | 146 | 333 | 402 | 7.62 | 501 | 38.74 | 128 | 344 | 410 | 5.42 | 602 | 680 | 7.38 |
| HTC-240-6 | 138 | 335 | 403 | 7.72 | 508 | 38.45 | 122 | 358 | 411 | 6.62 | 601 | 687 | 6.97 |
| HTC-240-12 | 146 | 331 | 400 | 7.38 | 512 | 39.52 | 131 | 342 | 409 | 6.04 | 602 | 701 | 6.99 |
| HTC-240-24 | 125 | 343 | 401 | 7.48 | 532 | 40.52 | 127 | 341 | 409 | 6.6 | 587 | 674 | 7.68 |
| HTC-40 % | 139 | 335 | 401 | 7.35 | 520 | 39.48 | 127 | 355 | 410 | 7.07 | 591 | 696 | 6.94 |
| HTC-60 % | 138 | 335 | 399 | 7.31 | 518 | 38.59 | 129 | 355 | 407 | 6.16 | 576 | 679 | 7.65 |
| HTC-80 % | 151 | 335 | 398 | 7.17 | 508 | 38.45 | 132 | 356 | 405 | 6.74 | 588 | 690 | 6.64 |

^a Increase in mass loss rate after the drying stage.

^b Temperature when the absolute mass loss is ~ 14 wt%.

^c Peak temperature at the highest mass loss rate.

^d Temperature when the absolute mass loss is ~ 50 wt%.

^e Residual mass (%) at the temperature of 900 °C.

^f Peak temperature at the highest mass loss rate in the devolatilization stage.

^g Peak temperature at the highest mass loss rate in the char combustion stage.

^h Burnout temperature.

guaiacol, methyl guaiacol, and ethyl guaiacol [109]. Ischia et al. [74] stated that phenolic compounds are the main products present in the liquid phase when lignin in hydrothermally treated at 320 °C. This formation of phenolic compounds is shown in the mass spectrometry analysis (section 3.4). Similarly, the main emission of CO₂, CO, and CH₄ takes place in this stage at temperatures close to 400 °C as a product of the rupture of C–C bonds promoted by the excision of β–O–4 bonds [110]. It should be noted that the rate of lignin decomposition can be improved, and its degradation temperature can be decreased by using catalysts that promote hydrolysis and depolymerization through selective cleavage of β–O–4 bonds in small fragments, altering the reaction pathways directly and modifying the hydrochar [52].

By stage III (>500 °C), approximately 50 wt% of the initial mass has reacted, representing an additional mass loss of roughly 11 %. At the end of the pyrolytic process, a solid residue of about 40 wt% remained in all samples due to the formation of highly condensed aromatic structures, which are the structures that form char when lignin is heated under oxidizing conditions.

Regarding the oxidative atmosphere, the first two stages corresponding to initial devolatilization (stage I) and main devolatilization (stage II), are like those at inert conditions, taking place in a similar range of temperatures (130–330 °C) and (330–460 °C), respectively. The release of light compounds enhances the devolatilization and combustion of the sample [111]. In oxidizing conditions, stage III (> 460 °C) corresponded to the release of higher molecular weight compounds, char formation, and subsequent combustion [36]. The maximum rate of weight loss resulted at temperatures between 580 and 600 °C for HC samples and 527 °C for raw IKL. All the samples showed a complete degradation at 700 °C, generating an almost total loss of the remaining mass of the pyrolytic stage.

The thermal stability of IKL in combustion conditions has increased after the HTC process. This is indicated by the decrease in the peak values of the DTG curve and the increase in the temperatures at which these maximum values take place in stage III. There was an increase in the temperature of the maximum degradation rate point, going from

527 °C for IKL to temperatures up to 612 °C for the hydrothermally treated samples, indicating an improvement in thermal stability due to the HTC treatment.

However, as the HTC temperature increased from 200 to 240 °C, there was a decrease in the temperature of the maximum degradation rate of the samples, indicating an increase in the reactivity of the HC when increasing the process temperature. Chen et al. [112] reported a similar behavior where the temperature of the highest decomposition rate was decreased in hydrochar produced above 240 °C from camellia husks, a high lignin content biomass [113]. This slight variation in thermal stability can be attributed to aspects such as demineralization processes and the different concentrations of functional groups and their bonds. Demineralization and reduction of the ash content in coal samples have been shown to affect the temperature of the maximum combustion rate, reducing this up to 62 °C [114]. It has been previously reported that the minerals inherent to the biomass influence its reactivity, having an inhibitory role [115,116]. Furthermore, the carbon matrix of HC generated at 200 °C is expected to have a higher content of C–C bonds that are part of their aromatic skeleton than those generated at higher temperatures, as depicted in the FTIR analysis on Supplementary Material A. Thus, the former has slightly higher thermal stability since, although it lost some volatile and inorganic components during HTC, it did not undergo a drastic decomposition [105].

There is no marked difference between the maximum decomposition rates and the temperature at which these took place when the process time was increased up to 12 h. The sample treated for 24 h had a decrease of approximately 14 °C in the temperature of the maximum degradation rate compared with the other samples (stage III), this being attributed to its lower fixed carbon content. Previous studies have shown that biomasses with a lower fixed carbon content have a maximum combustion rate at earlier temperatures [117,118]. Similar behavior was observed in the hydrochar produced when the process water was recirculated, with these having an average reduction in the maximum decomposition rate of almost 13 °C compared to all previous samples.

The temperatures of the maximum weight loss rate of IKL and HC

were similar to those reported for bituminous and anthracite coal, 535 °C and 621 °C, respectively [119]. The maximum degradation rate of the hydrochar was between 6.3 and 7.2 wt.%/min, this being greater than the maximum degradation rate for bituminous and anthracite coal, 4.80 and 5.27 wt.%/min, respectively [119]. In combustion processes, it is preferable that the solid fuel has a low degradation rate, indicating that the fuel has a higher carbon content, a higher C/O atomic ratio, and a more compact physical structure, thus making its combustion more efficient [120]. The residual mass of all samples was practically zero because of the low level of inorganic compounds.

3.4. Mass spectrometry

Lignin is a phenolic polymer, and a large number of its component fragments are difficult to dissolve and disperse in aqueous media when the temperature is not high. The formation of hydrochar in lignin occurs preferably by solid–solid conversion, producing polyaromatic carbon that will be fragmented during combustion reactions, giving rise to different species during its degradation. The identification of degradation compounds is a big challenge due to the overlapping of many signals. One *m/z* signal from the MS analysis can correspond to several fragmentation ions, or the fragmentation ion may come from different compounds [109]. The complex phenolic and polyaromatic hydrochar structure of lignin HTC products results in a significant number of chromatographic peaks. A total of 38 main compounds were identified based on literature reports for lignin degradation and pyrolysis [121–125]. The main extracted ion (EI) peaks characteristic of lignin degradation are shown in Table 5. The ion current intensities for the main identified components are listed in Table 2A. The components released for each of the selected samples under inert conditions were grouped by chemical families, Fig. 5.

From Fig. 5 the variation in the detection of different compounds for the IKL and the selected hydrochar samples can be observed. It can be observed from the inert atmosphere that the overall changes between the different groups of compounds are minor. However, small differences can be observed between the samples and the untreated IKL. Notably, as the temperature increased, the relative amount of guaiacol and phenolic compounds also increased. As mentioned in section 3.2, the hydrothermal process can lead to the breakdown of methyl (CH₃) and methylene (CH₂) groups in the aliphatic region of the guaiacyl units, resulting in the formation of guaiacols. This explains the difference between IKL and hydrochar, with the latter having a higher concentration of guaiacol-type compounds (i.e., guaiacol, methyl guaiacol, and ethyl guaiacol). Furthermore, the degradation of guaiacols through the fracture of their methoxy group (OCH₃) can lead to the formation of catechol-type phenolic compounds. This increase in catechol refers to demethylation mechanisms reactions. Moreover, the mild increase in the phenolic group may be attributed to rupture of β-ether bonds during hydrothermal process, as pointed out in section 3.3.

Although there is a similar trend regarding the greater presence of aromatic and phenolic compounds in hydrochar compared to IKL, there is a greater fluctuation of these groups when thermally decomposing them in an oxidative atmosphere. The presence of oxygen promotes oxidative reactions, leading to a higher degree of chemical transformation. Oxygen can reduce the energy barrier of the thermochemical reaction, enhancing the decomposition of organic materials, leading to more varied breakdown products and intermediate compounds [130]. This results in the formation and destruction of various compounds, leading to variations in their concentrations.

The profiles of the major chemical compounds in inert and oxidative atmospheres are shown in Fig. 6. Formation of guaiacols, phenols, diverse aromatics, and other compounds such as furfural, naphthalene, and acids were the most prominent products detected. As expected, the highest signal was reported for guaiacols in both atmospheres due to the softwood nature of the feedstock, which is composed mainly of G units with small quantities of H. The identified guaiacols are primarily

Table 5
Chemical compounds using extracted ion (EI) in MS analysis.

| Identification | Major contributing ions | | MS fragments | Ref. |
|------------------------------|-------------------------|--|----------------------|---------------|
| | EI | Structure | | |
| Guaiacols | | | | |
| Guaiacol | 124 | C ₇ H ₈ O ₂ | 109, 124, 81, 53, 82 | [121,123,125] |
| Methyl guaiacol | 123 | C ₈ H ₁₀ O ₂ | 138, 95, 77 | [122,123] |
| Ethyl guaiacol | 137 | C ₉ H ₁₂ O ₂ | 103,112, 122, 152 | [123–125] |
| Propyl guaiacol | 166 | C ₁₀ H ₁₄ O ₂ | 137, 122 | [125] |
| Vinyl guaiacol | 150 | C ₉ H ₁₀ O ₂ | 135, 107, 77 | [126] |
| Vanillin | 152 | C ₈ H ₈ O ₃ | 123, 109 | [125] |
| Eugenol | 164 | C ₁₀ H ₁₂ O ₂ | 149, 103 | [125] |
| Isoeugenol | 164 | C ₁₀ H ₁₂ O ₂ | 150, 104 | [125] |
| Hydroxy methoxy acetophenone | 149 | C ₉ H ₁₀ O ₃ | 125, 126 | [125] |
| Phenols | | | | |
| Phenol | 94 | C ₆ H ₆ O | 66, 65 | [123] |
| Alkylphenols | 107 | – | 121, 135 | [122] |
| Cresol | 108 | CH ₃ C ₆ H ₄ OH | 107, 108 | [123] |
| Ethyl phenol | 122 | C ₈ H ₁₀ O | 107, 77 | [123] |
| 4-(1-methyl ethyl)-phenol | 121 | C ₉ H ₁₂ O | 136, 150 | [127] |
| Dimethyl phenol | 122 | C ₈ H ₁₀ O | 107, 121 | [123] |
| C2-Alkylphenol | 122 | – | 107, 121 | [123] |
| 4-vinyl phenol | 120 | C ₈ H ₈ O | 91, 119 | [123] |
| Catechol | 110 | C ₆ H ₆ O ₂ | 66 | [128,129] |
| Methylcatechol | 123 | C ₇ H ₈ O ₂ | 124 | [122] |
| Ethyl catechol | 123 | C ₈ H ₁₀ O ₂ | 138, 77 | [122] |
| Aromatics | | | | |
| Benzene | 78 | C ₆ H ₆ | | [128] |
| Toluene | 92 | C ₇ H ₈ | | [128] |
| Ethylbenzene | 106 | C ₈ H ₁₀ | | [128] |
| Xylene | 106 | C ₈ H ₁₀ | | [128] |
| Styrene | 104 | C ₈ H ₈ | | [128] |
| hydroxy benzaldehyde | 121 | C ₇ H ₆ O ₂ | 122, 93, 65, 39 | [122] |
| Dihydroxy methylbenzene | 124 | C ₇ H ₈ O ₂ | | [123] |
| Indene | 116 | C ₉ H ₈ | | [128] |
| Other Compounds | | | | |
| Furfural | 96 | C ₅ H ₄ O ₂ | 95 | [129] |
| Propyne | 40 | C ₃ H ₄ | | [128] |
| Propene | 42 | C ₃ H ₆ | | [128] |
| Ketene | 42 | CH ₂ = CO | | [128] |
| Cyclopentadiene | 66 | C ₅ H ₆ | | [128] |
| 2-cyclopenten-1-one | 82 | C ₅ H ₆ O | | [128] |
| Naphthalene | 128 | C ₁₀ H ₈ | | [128] |
| 5-hydroxymethylfurfural | 126 | C ₆ H ₆ O ₃ | 97, 69 | [125] |
| Acetic acid | 60 | CH ₃ COOH | | [125] |
| Carboxylic acid | 45 | COOH+ | | [128] |

composed of guaiacol (EI 124), methyl guaiacol (MetG) (EI 123), propyl guaiacol (EI 166), and eugenol (EI 164), with the highest release at temperatures between 320–400 °C in an inert atmosphere and relatively constant release in an air atmosphere for the selected samples. In some samples, the release of guaiacol took place at lower temperatures compared to MetG, as in the case of sample HTC–200–6, where a temperature difference of approximately 50 °C between MetG and guaiacol was observed. This means that breaking C–H bonds on MetG had greater difficulty than on guaiacol [121]. Previous studies on lignin pyrolysis have pointed out that the formation of these compounds and their occurrence temperature highly depend on the lignin type itself. In particular, Brebu et al. [109] evaluated the thermal degradation of Klason, organosolv and kraft lignin, identifying changes in the temperatures at which various compounds are detected during pyrolysis. The most significant temperature change was observed for Klason lignin,

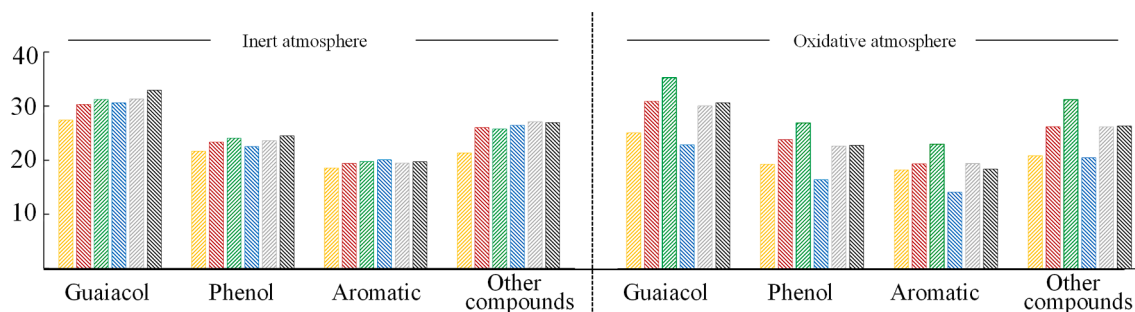


Fig. 5. Production of classified chemical compounds of studied samples and IKL in mass spectrometry.

with a difference of approximately 100 °C between the occurrences of guaiacol and ethylguaiacol. On the other hand, the formation of guaiacol homologs occurred simultaneously for softwood kraft lignin, which is consistent with the observations in the present study. As shown in Fig. 6, the occurrence temperatures of guaiacol and MetG for each of the samples are similar, suggesting that originated from one polymeric structure. In softwood, it is known that lignin in different morphological parts has a structurally homogeneous composition, which can influence its degradation pattern.

The release of phenols showed similar behavior to that of guaiacols, with maximum release temperatures around 400 °C under an inert atmosphere. It should be noted that kraft lignins have increased the content of free phenolic groups and of C–C linkages due to structural changes occurring during the pulping process [109]. Phenols are associated with secondary reactions of lignin at temperatures of 400–600 °C, derived from the cracking of bonded hydroxyl- and methoxy-phenylpropane units of lignin [131,132]. Soongpravit et al. [131] indicated a higher selectivity for the formation of methoxy phenol and alkylated phenol during lignin pyrolysis in this range of temperature. Likewise, it is mentioned that high pyrolytic temperatures may lead to a reduction of phenolic compounds due to thermal fragmentation of the C–C linkage in the aromatic structure. Under oxidative conditions, the release of alkylphenol seemed to occur in two steps in the recirculating sample, where there was first high release at temperatures around 150 °C and then release increased again at temperatures around 600 °C. The detection of these aromatics in the early stages of the process could represent the release of phenolic compounds absorbed by the HC. The high amount of phenolic and aromatic compounds released in the recirculation samples could be related to the analysis of section 3.2, where a higher mass yield was obtained for these samples compared to non-recirculated samples. Moreover, it can be seen from Fig. 5, where the recirculation samples show a higher presence of phenolic groups. It is possible that the lignin fragments dissolved in the aqueous medium (fragments that would be decomposed to phenolic compounds through hydrolytic reactions) were transformed into phenolic carbon and then located on the non-dissolved lignin surface. Likewise, it was possible that an adsorption/desorption effect of the dissolved fragments may be taking place in the hydrochar matrix, as indicated in previous studies. For instance, Ischia et al. [99] conducted extraction using various solvents on HTC-derived hydrochar, finding that the composition of the extracted species resembles that of the HTC liquors. The similarity between the extract and the liquor compositions suggests that these extracted compounds come from the liquor itself and are absorbed on the surface of the hydrochar during the HTC process. Moreover, it is pointed out that solvent extraction does not selectively remove compounds based on functional groups, thus indicating that the adsorption of the compounds to the hydrochar is physical in nature given this desorption.

Naphthalene showed an apparent constant formation in the oxidizing atmosphere, with higher detection for sample HTC–240–6 at 300 °C. The opposite occurs under inert conditions, where in the sample treated at 200 °C, the detection of naphthalene increased as the

temperature increased. In the samples treated at 240 °C, the amount of naphthalene released decreased as the temperature increased. At higher temperatures, a better dissociation of the aromatic compounds present in the lignin structure was achieved. Naphthalene was found to be the dominant product from lignin degradation under catalytic pyrolysis, as reported by [133]. In the pyrolytic process, naphthalene and indene are generally the main polycyclic aromatics detected.

The carboxylic acids obtained by deprotonation of the carboxyl group can be assigned to guaiacols. Additionally, carboxylic acid can be generated during the depolymerization of lignin to phenols and aldehydes, whose formation is increased or promoted at high temperatures [134]. The highest release of carboxylic acid was at temperatures close to 600 °C. The highest peak was found for HTC–80 % and HTC–40 % under inert and oxidative atmospheres, respectively. Acetic acid was one of the major compounds found in most of the samples. The maximum detection of acetic acid occurs at temperatures between 350 and 400 °C, with lower detection at 700 °C for all samples. Its formation was related to the cleavage of carbon acetylated in the lignin side chain [135]. Additionally, and like furfurals, the release of these organic groups in the lignin hydrochar pyrolysis results mainly from the cracking and reforming of the ether groups [121].

3.5. Simulation results

The process design for the industrial-scale lignin HTC treatment plant was based on the case of 220 °C temperature, 6 h residence time, 9:1 ratio of water to dry matter, and no recirculation of the liquid. The 9:1 water-to-dry ratio is achieved with the addition of 16.4 kg/s of liquid water, as well as 1.5 kg/s of 25 bar steam for reactor heating, to 30 % wet-basis moisture content lignin, for a 5.5:1 mass ratio of added water to wet-basis lignin feedstock. 30 % is often cited for kraft lignin moisture before dewatering [136,137], although some references to ranges of 30–35 % [138] or even up to 40 % [139] also exist. The demand for water is not sensitive to feedstock moisture: liquid water addition remains at 16–17 kg/s range with 10–60 % lignin moisture.

Not recirculating the liquids was chosen on the grounds of this achieving the highest mass yield of the product. Although higher temperatures and residence times would yield somewhat higher HHV of the final product, the difference would be small. At the same time, there would be a significant cost for increased temperatures or residence times: higher temperatures could not be achieved with extraction steam, necessitating the use of main steam for final heating and thereby considerable power generation penalty and the larger volumes of pressure vessels needed for processing the same rates of lignin at longer residence times would require larger pressure vessels with thicker walls, for significant investment cost increase.

The main results for integrating an HTC treatment plant processing 7.5 t/h of dry lignin are listed in Table 6. A similar amount of lignin removal without the HTC treatment is also included for comparison purposes. It is evident from the results that the main impacts on the boiler and steam cycle are due to the lignin removal itself and the consequent reduction of boiler fuel input; the addition of the HTC

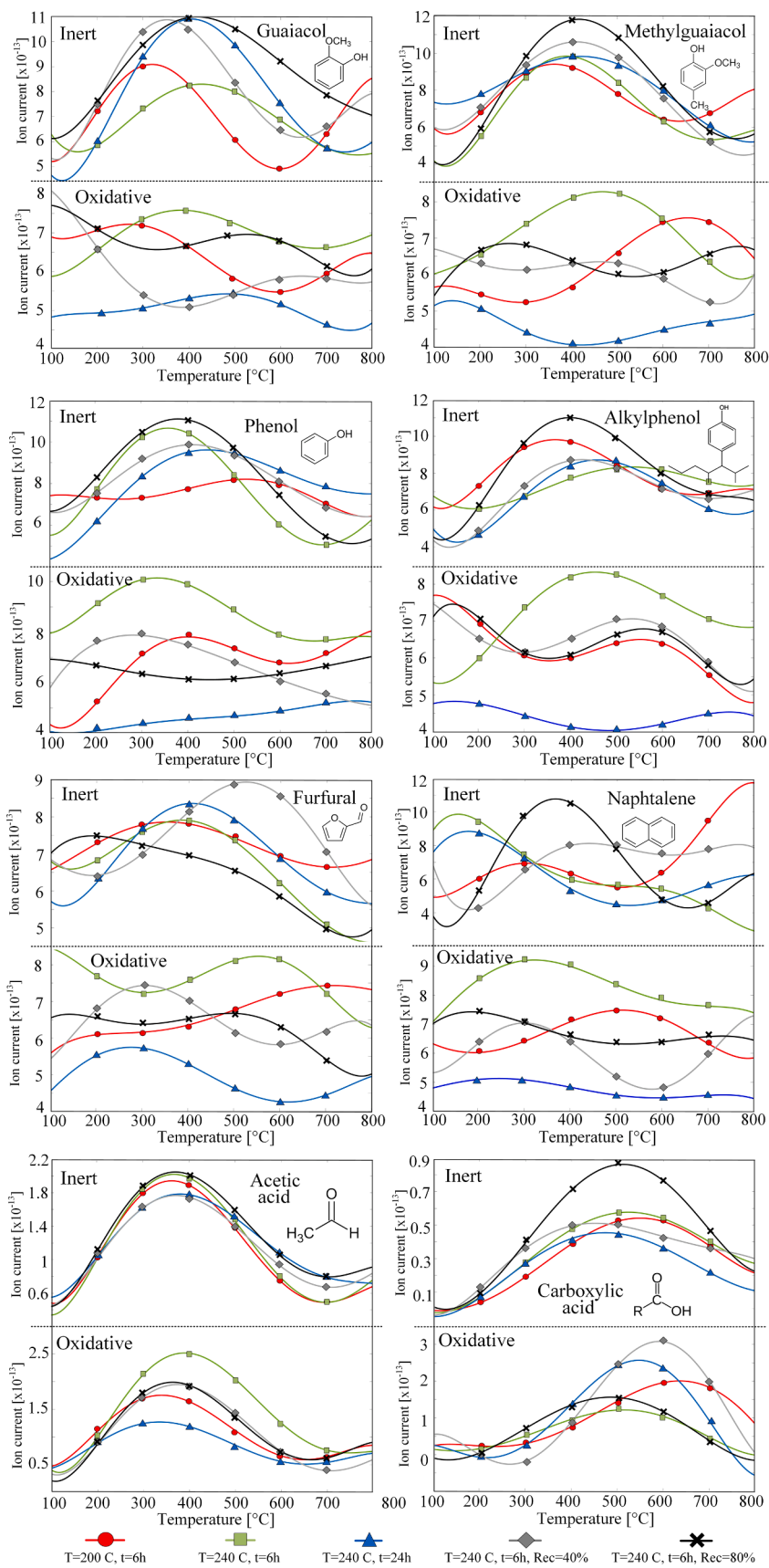


Fig. 6. Profiles of chemical compound production fractionated by mass spectrometry.

Table 6
Lignin removal (LR) and HTC treatment impact on power and steam generation.

| | Parameter | 0 | LR | LR + HTC | |
|--|---|--|-------------|-------------|---------|
| Boiler | Firing liquor input, kg _{ds} /s | 88.09 | 85.88 | 85.88 | |
| | Firing liquor lignin, kg _{lig} /kg _{ds} | 0.310 | 0.293 | 0.293 | |
| | Firing liquor HHV, MJ/kg | 13.16 | 12.91 | 12.91 | |
| | Firing liquor energy, MW _{LHV+sensible} | 1085.9 | 1038.8 | 1038.8 | |
| | Main steam values, °C/bar | 510 / 100 | 510 / 100 | 510 / 100 | |
| | Main steam production, kg/s | 333.5 | 316.3 | 316.2 | |
| | Lignin removal and HTC | Lignin removal, kg _d /s | 0 | 2.08 | 2.08 |
| Lignin final moisture, wt.% | | <i>n/a</i> | 10 | 30 | |
| Hydrochar production, kg _d /s | | <i>n/a</i> | <i>n/a</i> | 1.96 | |
| Hydrochar final moisture, wt.% | | <i>n/a</i> | <i>n/a</i> | 10 | |
| Steam from backpressure turbine | 27 bar HP extraction, kg/s (bar) | 17.3 (27.0) | 17.3 (25.5) | 18.8 (25.5) | |
| | 12 bar MP extraction, kg/s (bar) | 86.2 (12.0) | 83.7 (11.4) | 83.6 (11.3) | |
| | 5 bar LP extraction ^a , kg/s (bar) | 179.4 (5.0) | 178.9 (5.0) | 177.2 (5.0) | |
| | Condensing turbine, kg/s (bar) | 48.8 (4.60) | 35.9 (3.38) | 35.2 (3.32) | |
| | Deaerator heating ^b , kg/s (bar) | 48.54 (4.2) | 46.1 (4.2) | 44.8 (4.2) | |
| | Power generation and consumption | Gross generator power, MW _{el} | 213.710 | 193.942 | 193.055 |
| | | Boiler and steam cycle auxiliaries, MW _{el} | 7.258 | 6.805 | 6.811 |
| Pulp mill power consumption, MW _{el} | | 60.375 | 60.375 | 60.375 | |
| Lignin removal power consumption, MW _{el} | | 0 | 0.600 | 0.150 | |
| HTC power consumption, MW _{el} | | 0 | 0 | 0.659 | |
| Net power available to sell, MW _{el} | | 146.077 | 126.163 | 125.060 | |

^a LP steam pressure maintained by condensing turbine throttling valve.

^b Deaerator heating steam included in LP extraction steam.

process imparts a relatively minor impact to this. The reductions of high (HP) and medium (MP) steam extraction pressures remain small, corresponding to only 2–3 °C saturation temperature reduction. This small reduction was considered unlikely to cause problems for steam users. LP pressure is maintained at 5 bar by throttling the condensing turbine inlet flow. Main steam parameters can still be maintained for the main steam at this level of fuel power reduction; with lignin removal, attemperation spray still reduces temperature by 39 °C (68 °C in the base case).

In the case of only lignin removal, the thermal dryer heat demand is supplied from the plant's 5 bar LP steam. In the case of the HTC treatment plant, the raw lignin is pressed to MC = 30 % during the process of removing the black liquor residues from the lignin but not thermally dried, as more water must be added in any case for the HTC process. In the HTC treatment case, the final thermal drying of the hydrochar takes place with the hot wastewater from the HTC process; this is sufficient to achieve the 10 % final moisture without the need for additional steam from the plant.

The HTC plant scheme is depicted in Fig. 7. In contrast to the HTC

plant schemes of [65] and, where the hot wastewater from the dewatering was used as part of the water supply for the feed slurry, and direct injection of flash vapor from product slurry depressurization was used for both heat recovery and reducing the water consumption and wastewater production, in this case, no recirculation is used in order to maximize the product mass yield. In addition to the improved mass yield, this has the advantage of simplified feed slurry pressurization, which can now be achieved with a single slurry pump without the need to pressurize in stages to maintain a pressure gradient from the flash tanks to the feed. The disadvantages are increased water consumption and the need for indirect heating of the slurry in condensing heat exchangers, as opposed to direct flash vapor injection. The former amounts to a relatively small additional expense [140], however, while the latter is less of a problem in the case of a high-water-content slurry with very fine lignin particles, as opposed to the much larger particle sizes and somewhat lower water contents considered in the aforementioned studies, where fouling and clogging of heat exchangers could be expected to be a significant risk.

The feed heating consists of 5 separate stages; first, the 15 °C raw water is heated to 34 °C with hot wastewater from product slurry dewatering and the condensing slurry heaters; after mixing the water and the lignin and pressurizing to 28 bar in a slurry pump, the slurry is heated to 93 °C in the first condensing heater using 1 bar flash vapor. This is followed by a second heater using 5 bar LP steam from the plant (3.8 MW) for 143 °C temperature, and then a 12 bar flash vapor heater for a 181 °C slurry temperature entering the reactor, which is heated with 4.6 MW of 25.4 bar HP steam to the final temperature of 220 °C. A 3.4 MW excess of 1 bar flash steam is used to preheat the demineralized makeup water for the mill; this results in reduced deaerator steam consumption, as seen in Table 6, and a net outcome of similar condensing turbine flow and inlet pressure as would be achieved without the HTC plant.

4. Conclusions and suggestions

This study has shown that the hydrothermal process, under the evaluated experimental conditions, led to moderate changes in IKL. Among the operational parameters, temperature and time had the greatest influence on the process outcome, while process water recirculation had a lesser impact. Increasing temperature and time resulted in slight decreases in mass yield and volatile matter. However, extended residence times (up to 24 h) and recirculation, increased volatile matter, likely due to re-absorption of aqueous phase degradation products. Recirculation also showed increased mass yield with higher concentrations of process water. Hydrochar produced at 240 °C for 6 h without recirculation had higher fuel ratio and higher heating value. Extended reaction times did not significantly alter HHV. Minor changes in elemental carbon were noted with varying temperatures and times, alongside a noticeable reduction in hydrogen content, leading to a relative elevated oxygen content in hydrochar. This hydrogen reduction is attributed to both the cleavage of hydrogen-containing groups by demethylation reaction mechanisms and the formation of free radicals, which increase the content of oxygen functional groups on the hydrochar surface.

The slight general degradation of IKL was attributed to its recalcitrant nature, corroborated by thermogravimetric analysis indicating high thermal stability. Hydrothermal treatment induced minimal structural changes in IKL, resulting in subtle variations in thermal degradation profiles among hydrochar samples. Despite hydrochar and IKL exhibiting similar maximum weight loss rates near 400 °C, the rate of weight loss was slightly higher for hydrochar. During thermal degradation were identified various compounds, as guaiacol and phenolic aromatics, with a slightly greater presence in hydrochar due to changes in lignin structure. The higher presence of these compounds in recirculation samples was attributed to their adsorption from the liquid phase and not to a greater degradation of the initial sample. To have

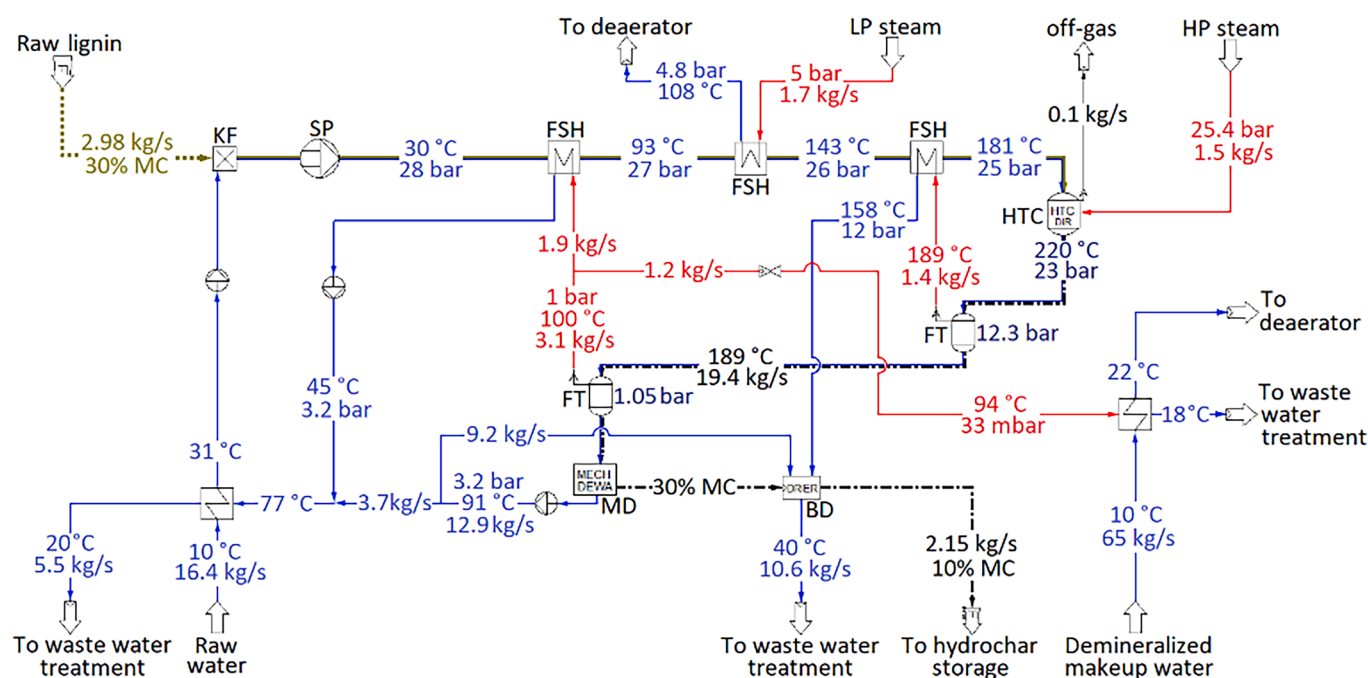


Fig. 7. Flowsheet model of the industrial-scale HTC process. KF – Kamyrr feeder; SP – slurry pump; FSH – feed slurry heater; HTC – HTC reactor; FT – flash tank; MD – mechanical dewatering; BD – belt drier.

greater degradation of the IKL during the hydrothermal process and obtain a hydrochar with higher carbon content, greater aromaticity and greater calorific value, it is necessary to carry out the HTC at higher temperatures.

The HTC process design and integration with the pulp mill recovery boiler and power plant was based on a 7.5 td/h scale. The simulation results showed that the largest energy impact occurs in the boiler due to removing lignin from the black liquor, which reduces the power output by 20 MW. The addition of a hydrothermal carbonization unit would further reduce this by only approximately 1 MW. Future work should focus on a comprehensive technical–economic evaluation for the integration of HTC lignin treatment to a pulp mill recovery boiler steam cycle to determine its feasibility on an industrial scale. Such evaluation should consider the effects of different process parameters such as higher operational temperatures and plant configurations on the economic performance.

Funding

This study was funded by project No.101092257, “Valorisation of CO₂ waste streams into polyester for a sustainable circular textile industry (THREADING-CO₂)”.

CRedit authorship contribution statement

Orlando Salcedo-Puerto: . **Clara Mendoza-Martinez**: Writing – review & editing, Writing – original draft, Visualization, Validation, Supervision, Methodology, Investigation, Conceptualization. **Jussi Saari**: Writing – review & editing, Software, Methodology, Investigation, Conceptualization. **Esa Vakkilainen**: Writing – review & editing, Validation, Supervision, Conceptualization.

Declaration of competing interest

The authors declare that they have no known competing financial interests or personal relationships that could have appeared to influence the work reported in this paper.

Data availability

Data will be made available on request.

Acknowledgments

The authors gratefully acknowledge Peter Jones’s support in improving the English language.

Appendix A. Supplementary data

Supplementary data to this article can be found online at <https://doi.org/10.1016/j.fuel.2024.132389>.

References

- [1] Huang J, Fu S, Gan L. Lignin chemistry and applications. Elsevier 2019. <https://doi.org/10.1016/B978-0-12-813941-7.00001-1>.
- [2] Sameni J, Krigstin S, dos Rosa S, Leao A, Sain M. Thermal characteristics of lignin residue from industrial processes. *BioResources* 2014;9:725–37. <https://doi.org/10.15376/biores.9.1.725-737>.
- [3] Demuner IF, Borges Gomes FJ, Gomes JS, Coura MR, Borges FP, Macedo Ladeira Carvalho AM, et al. Improving kraft pulp mill sustainability by lignosulfonates production from processes residues. *J Clean Prod* 2021;317:128286. <https://doi.org/10.1016/J.JCLEPRO.2021.128286>.
- [4] Atta-Obeng E, Dawson-Andoh B, Seehra MS, Geddam U, Poston J, Leisen J. Physico-chemical characterization of carbons produced from technical lignin by sub-critical hydrothermal carbonization. *Biomass Bioenergy* 2017;107:172–81. <https://doi.org/10.1016/j.biombioe.2017.09.023>.
- [5] Vishtal A, Kraslawski A. Challenges in industrial applications of technical lignins. *BioResources* 2011;6:3547–68. <https://doi.org/10.15376/biores.6.3.vishtal>.
- [6] Bajwa DS, Pourhashem G, Ullah AH, Bajwa SG. A concise review of current lignin production, applications, products and their environmental impact. *Ind Crops Prod* 2019;139:111526. <https://doi.org/10.1016/J.INDCROP.2019.111526>.
- [7] Chio C, Sain M, Qin W. Lignin utilization: a review of lignin depolymerization from various aspects. *Renew Sustain Energy Rev* 2019;107:232–49. <https://doi.org/10.1016/J.RSER.2019.03.008>.
- [8] Kawamoto H. Lignin pyrolysis reactions. *J Wood Sci* 2017;63:117–32. <https://doi.org/10.1007/S10086-016-1606-Z>.
- [9] Zheng X, Zhong Z, Zhang B, Du H, Wang W, Li Q, et al. Preparation of monocyclic aromatic hydrocarbons from industrial lignin residue and polyethylene copolymerization by microwave-assisted in fluidized bed based on bimetal-loaded HZSM-5/MCM-41 core-shell catalyst. *Fuel* 2024;364:131100. <https://doi.org/10.1016/J.FUEL.2024.131100>.

- [10] Li H, Liang Y, Li P, He C. Conversion of biomass lignin to high-value polyurethane: a review. *J. Bioresour. Bioprod.* 2020;5:163–79. <https://doi.org/10.1016/j.jobab.2020.07.002>.
- [11] Huang M, Xu J, Ma Z, Yang Y, Zhou B, Wu C, et al. Bio-BTX production from the shape selective catalytic fast pyrolysis of lignin using different zeolite catalysts: relevance between the chemical structure and the yield of bio-BTX. *Fuel Process Technol* 2021;216:106792. <https://doi.org/10.1016/j.fuproc.2021.106792>.
- [12] Deng J, Sun SF, Zhu EQ, Yang J, Yang HY, Wang DW, et al. Sub-micro and nano-lignin materials: small size and rapid progress. *Ind Crops Prod* 2021;164:113412. <https://doi.org/10.1016/j.indcrop.2021.113412>.
- [13] Matsakas L, Karnaouri A, Cwirzen A, Rova U, Christakopoulos P, Xu C, et al. Formation of Lignin Nanoparticles by Combining Organosolv Pretreatment of Birch Biomass and Homogenization Processes n.d. Doi: 10.3390/molecules23071822.
- [14] Petrie FA, Gorham JM, Busch RT, Leontsev SO, Ureña-Benavides EE, Vasquez ES. Facile fabrication and characterization of kraft lignin@Fe3O4 nanocomposites using pH driven precipitation: effects on increasing lignin content. *Int J Biol Macromol* 2021;181:313–21. <https://doi.org/10.1016/j.ijbiomac.2021.03.105>.
- [15] Venkatesan Savunthari K, Arunagiri D, Shanmugam S, Ganesan S, Arasu MV, Al-Dhabi NA, et al. Green synthesis of lignin nanorods/g-C3N4 nanocomposite materials for efficient photocatalytic degradation of triclosan in environmental water. *Chemosphere* 2021;272:129801. <https://doi.org/10.1016/j.chemosphere.2021.129801>.
- [16] Bourbiaux D, Pu J, Rataboul F, Djakovitch L, Geantet C, Laurenti D. Reductive or oxidative catalytic lignin depolymerization: an overview of recent advances. *Catal Today* 2021;373:24–37. <https://doi.org/10.1016/j.cattod.2021.03.027>.
- [17] Nguyen LT, Phan DP, Sarwar A, Tran MH, Lee OK, Lee EY. Valorization of industrial lignin to value-added chemicals by chemical depolymerization and biological conversion. *Ind Crops Prod* 2021;161:113219. <https://doi.org/10.1016/j.indcrop.2020.113219>.
- [18] Yaguchi AL, Lee SJ, Blenner MA. Synthetic biology towards engineering microbial lignin biotransformation. *Trends Biotechnol* 2021. <https://doi.org/10.1016/j.tibtech.2021.02.003>.
- [19] Chalewlerit-Umpun S, Liedel C. More sustainable energy storage: LIGNIN based electrodes with glyoxal crosslinking. *J Mater Chem A Mater* 2017;5:24344–52. <https://doi.org/10.1039/C7TA07686J>.
- [20] Liu H, Xu T, Liu K, Zhang M, Liu W, Li H, et al. Lignin-based electrodes for energy storage application. *Ind Crops Prod* 2021;165:113425. <https://doi.org/10.1016/j.indcrop.2021.113425>.
- [21] Cao M, Cheng W, Ni X, Hu Y, Han G. Lignin-based multi-channels carbon nanofibers @ SnO2 nanocomposites for high-performance supercapacitors. *Electrochim Acta* 2020;345:136172. <https://doi.org/10.1016/j.electrochim.2020.136172>.
- [22] Yoganandham ST, Sathyamoorthy G, Renuka RR. Emerging extraction techniques : Hydrothermal processing. *Sustainable Seaweed Technologies*. Elsevier Inc.; 2020. p. 191–205.
- [23] Lu X. Understanding hydrothermal carbonization of mixed feedstocks for waste conversion. University of South Carolina; 2014. Doctoral dissertation).
- [24] Kirtania K. Thermochemical conversion processes for waste bio refinery. *Waste Biorefinery: potential and Perspectives*. Elsevier B.V.; 2018. p. 129–56.
- [25] Dinjus E, Kruse A, Tröger N. Hydrothermal carbonization - 1. Influence of lignin in lignocelluloses. *Chem Eng Technol* 2011;34:2037–43. <https://doi.org/10.1002/ceat.201100487>.
- [26] Libra JA, Ro KS, Kammann C, Funke A, Berge ND, Neubauer Y, et al. Hydrothermal carbonization of biomass residuals: a comparative review of the chemistry, processes and applications of wet and dry pyrolysis. *Biofuels* 2011;2:71–106. <https://doi.org/10.4155/bfs.10.81>.
- [27] Reza MT, Rottler E, Herklotz L, Wirth B. Hydrothermal carbonization (HTC) of wheat straw: influence of feedwater pH prepared by acetic acid and potassium hydroxide. *Bioresour Technol* 2015;182:336–44. <https://doi.org/10.1016/j.biortech.2015.02.024>.
- [28] Román S, Nabais JMV, Laginhas C, Ledesma B, González JF. Hydrothermal carbonization as an effective way of densifying the energy content of biomass. *Fuel Process Technol* 2012;103:78–83. <https://doi.org/10.1016/j.fuproc.2011.11.009>.
- [29] Mendoza Martinez CL, Sermyagina E, Saari J, Silva de Jesus M, Cardoso M, Matheus de Almeida G, et al. Hydrothermal carbonization of lignocellulosic agro-forest based biomass residues. *Biomass Bioenergy* 2021;147:106004. <https://doi.org/10.1016/j.biombioe.2021.106004>.
- [30] Pawlak-Kruczek H, Niedzwiecki L, Sieradzka M, Mlonka-Mędrala A, Baranowski M, Serafin-Tkaczuk M, et al. Hydrothermal carbonization of agricultural and municipal solid waste digestates – Structure and energetic properties of the solid products. *Fuel* 2020;275:117837. <https://doi.org/10.1016/j.fuel.2020.117837>.
- [31] Erses Yay AS, Birinci B, Açıklan S, Yay K. Hydrothermal carbonization of olive pomace and determining the environmental impacts of post-process products. *J Clean Prod* 2021;315:128087. <https://doi.org/10.1016/j.jclepro.2021.128087>.
- [32] Paini J, Benedetti V, Menin L, Baratieri M, Patuzzi F. Subcritical Water Hydrolysis coupled with Hydrothermal Carbonization for apple pomace integrated cascade valorization. *Bioresour Technol* 2021;125956. <https://doi.org/10.1016/j.biortech.2021.125956>.
- [33] Kızılduman BK, Turhan Y, Doğan M. Mesoporous carbon spheres produced by hydrothermal carbonization from rice husk: optimization, characterization and hydrogen storage. *Adv Powder Technol* 2021. <https://doi.org/10.1016/j.appt.2021.09.025>.
- [34] Fitri Faradilla RH, Lucia L, Hakovirta M. Hydrothermal carbonization of soybean hulls for the generation of hydrochar: a promising valorization pathway for low value biomass. *Environ Nanotechnol Monit Manag* 2021;16:100571. <https://doi.org/10.1016/j.enmm.2021.100571>.
- [35] Wilk M, Śliz M, Gajek M. The effects of hydrothermal carbonization operating parameters on high-value hydrochar derived from beet pulp. *Renew Energy* 2021;177:216–28. <https://doi.org/10.1016/j.renene.2021.05.112>.
- [36] Sermyagina E, Mendoza C, Deviatkin I. Effect of hydrothermal carbonization and torrefaction on spent coffee grounds. *Agron Res* 2021;19:928–43. <https://doi.org/10.15159/ar.21.023>.
- [37] Huezo L, Vasco-Correa J, Shah A. Hydrothermal carbonization of anaerobically digested sewage sludge for hydrochar production. *Bioresour Technol Rep* 2021;15:100795. <https://doi.org/10.1016/j.biteb.2021.100795>.
- [38] Wilk M, Śliz M, Lubieniecki B. Hydrothermal co-carbonization of sewage sludge and fuel additives: combustion performance of hydrochar. *Renew Energy* 2021;178:1046–56. <https://doi.org/10.1016/j.renene.2021.06.101>.
- [39] Ma XQ, Liao JJ, Chen DB, Xu ZX. Hydrothermal carbonization of sewage sludge: catalytic effect of Cl⁻ on hydrochars physicochemical properties. *Mol Catal* 2021;513:111789. <https://doi.org/10.1016/j.mcat.2021.111789>.
- [40] Mendoza Martinez CL, Sermyagina E, Vakkilainen E. Hydrothermal Carbonization of Chemical and Biological Pulp Mill Sludges. *Energies* 2021, Vol 14, Page 5693 2021;14:5693. Doi: 10.3390/EN14185693.
- [41] Hu B, Wang K, Wu L, Yu S-H, Antonietti M, Titirici M-M. Engineering carbon materials from the hydrothermal carbonization process of biomass. *Adv Mater* 2010;22:813–28. <https://doi.org/10.1002/adma.200902812>.
- [42] Kruse A, Funke A, Titirici MM. Hydrothermal conversion of biomass to fuels and energetic materials. *Curr Opin Chem Biol* 2013;17:515–21. <https://doi.org/10.1016/j.cbpa.2013.05.004>.
- [43] Kim D, Lee K, Park KY. Upgrading the characteristics of biochar from cellulose, lignin, and xylan for solid biofuel production from biomass by hydrothermal carbonization. *J Ind Eng Chem* 2016;42:95–100. <https://doi.org/10.1016/j.jiec.2016.07.037>.
- [44] Wikberg H, Ohra-Aho T, Pileidis F, Titirici MM. Structural and morphological changes in kraft lignin during hydrothermal carbonization. *ACS Sustain Chem Eng* 2015;3:2737–45. <https://doi.org/10.1021/acsuschemeng.5b00925>.
- [45] Sangchoom W, Mokaya R. Valorization of lignin waste: carbons from hydrothermal carbonization of renewable lignin as superior sorbents for CO2 and hydrogen storage. *ACS Sustain Chem Eng* 2015;3:1658–67. <https://doi.org/10.1021/acsuschemeng.5b00351>.
- [46] Mao H, Chen X, Huang R, Chen M, Yang R, Lan P, et al. Fast preparation of carbon spheres from enzymatic hydrolysis lignin: effects of hydrothermal carbonization conditions. *Sci Rep* 2018;8:2–11. <https://doi.org/10.1038/s41598-018-27777-4>.
- [47] Leng S, Leng L, Chen L, Chen J, Chen J, Zhou W. The effect of aqueous phase recirculation on hydrothermal liquefaction/carbonization of biomass: a review. *Bioresour Technol* 2020;318:124081. <https://doi.org/10.1016/j.biortech.2020.124081>.
- [48] He M, Zhu X, Dutta S, Khanal SK, Lee KT, Masek O, et al. Catalytic co-hydrothermal carbonization of food waste digestate and yard waste for energy application and nutrient recovery. *Bioresour Technol* 2022;344:126395. <https://doi.org/10.1016/j.biortech.2021.126395>.
- [49] He M, Cao Y, Xu Z, You S, Ruan R, Gao B, et al. Process water recirculation for catalytic hydrothermal carbonization of anaerobic digestate: water-Energy-Nutrient Nexus. *Bioresour Technol* 2022;361:127694. <https://doi.org/10.1016/j.biortech.2022.127694>.
- [50] Zaccariello L, Battaglia D, Morrone B, Mastellone ML. Hydrothermal carbonization: a pilot-scale reactor design for bio-waste and sludge pre-treatment. *Waste Biomass Valorization* 2022;13:3865–76. <https://doi.org/10.1007/s12649-022-01859-X/TABLES/9>.
- [51] Miikka Veikkolainen. Implementation of the HTC Plant as Part of Wastewater Treatment at Stora Enso Heinola Fluting Mill. 2022.
- [52] Cao Y, He M, Dutta S, Luo G, Zhang S, Tsang DCW. Hydrothermal carbonization and liquefaction for sustainable production of hydrochar and aromatics. *Renew Sustain Energy Rev* 2021;152:111722. <https://doi.org/10.1016/j.rser.2021.111722>.
- [53] Cao Y, Zhang C, Tsang DCW, Fan J, Clark JH, Zhang S. Hydrothermal liquefaction of lignin to aromatic chemicals: impact of lignin structure. *Ind Eng Chem Res* 2020;59:16957–69. https://doi.org/10.1021/ACS.IECR.0C01617/SUPPL_FILE/IEC01617_SI_001.PDF.
- [54] Sfs. en iso. 18134-2 Solid biofuels. determination of moisture content. Part 2: Simplified method 2024.
- [55] SFS. EN 15148 Solid biofuels. Determination of the content of volatile matter. 2012.
- [56] SFS. EN 14775 Solid biofuels. Determination of ash content 2009.
- [57] Sfs. en. 14918 Solid biofuels. Determination of calorific value 2012.
- [58] Sfs. iso. 16948 Solid biofuels. Determination of total content of carbon, hydrogen and nitrogen 2015.
- [59] SFS. EN ISO 16994 Solid biofuels. Determination of total content of sulfur and chlorine 2016.
- [60] Flynn JH, Wall LA. General treatment of the thermogravimetry of polymers. *J Res Natl Bur Stand A Phys Chem* 1966;70A:487. <https://doi.org/10.6028/jres.070a.043>.
- [61] Ozawa T. A new method of analyzing thermogravimetric data. *Bull Chem Soc Jpn* 1965;38:1881–6. <https://doi.org/10.1246/bcsj.38.1881>.
- [62] Akahira T, Sunose T. Method of determining activation deterioration constant of electrical insulating materials. *Res Rep Chiba Inst Technol (Sci Technol)* 1971;16:22–31.

- [63] Kissinger HE. Reaction kinetics in differential thermal analysis. *Anal Chem* 1957; 29:1702–6. <https://doi.org/10.1021/ac60131a045>.
- [64] Friedman HL. Kinetics of thermal degradation of char-forming plastics from thermogravimetry. application to a phenolic plastic. *J Polym Sci, Part C: Polym Symp* 2007. <https://doi.org/10.1002/polc.5070060121>.
- [65] Saari J, Sermiyagina E, Kaikko J, Haider M, Hamaguchi M, Vakkilainen EK. Evaluation of the Energy Efficiency Improvement Potential through Back-End Heat Recovery in the Kraft Recovery Boiler. *Energies* 2021, Vol 14, Page 1550 2021;14:1550. Doi: 10.3390/EN14061550.
- [66] Hamaguchi M, Kautto J, Vakkilainen EK. Effects of hemicellulose extraction on the kraft pulp mill operation and energy use: review and case study with lignin removal. *Chem Eng Res Des* 2013;91:1284–91. <https://doi.org/10.1016/j.cherd.2013.02.006>.
- [67] Saari J, Kuparinen K, Sermiyagina E, Vakkilainen EK, Kaikko J, Sergeev V. Effect of integration method and carbonization temperature on the performance of an integrated hydrothermal carbonization and CHP plant. *BioResources* 2018;13: 5080–110. <https://doi.org/10.15376/biores.13.3.5080-5110>.
- [68] Kuparinen K, Vakkilainen E. Green pulp mill: renewable alternatives to fossil fuels in lime kiln operations. *BioResources* 2017;12:4031–48. <https://doi.org/10.15376/BIORES.12.2.4031-4048>.
- [69] T. Weng W.A. Yee geotextile tube contribution to carbon footprint savings at Tianjin Eco-City 2014 China.
- [70] Vakkilainen EK. *Solid Biofuels and Combustion. Steam Generation from Biomass: Lappeenranta, Finland; 2017. p. 18–56.*
- [71] Niu Y, Tan H, Hui S. Ash-related issues during biomass combustion: alkali-induced slagging, silicate melt-induced clumping (ash fusion), agglomeration, corrosion, ash utilization, and related countermeasures. *Prog Energy Combust Sci* 2016;52:1–61. <https://doi.org/10.1016/j.peccs.2015.09.003>.
- [72] Wang F, Wang J, Gu C, Han Y, Zan S, Wu S. Effects of process water recirculation on solid and liquid products from hydrothermal carbonization of *Laminaria*. *Bioresour Technol* 2019;292:121996. <https://doi.org/10.1016/j.biortech.2019.121996>.
- [73] Wüst D, Correa CR, Jung D, Zimmermann M, Kruse A, Fiori L. Understanding the influence of biomass particle size and reaction medium on the formation pathways of hydrochar. *Biomass Conversion and Biorefinery* 2019 10:4 2019;10: 1357–80. Doi: 10.1007/S13399-019-00488-0.
- [74] Ischia G, Sudiby H, Miotello A, Tester JW, Fiori L, Goldfarb JL. Identifying the transition from hydrothermal carbonization to liquefaction of biomass in a batch system. *ACS Sustain Chem Eng* 2024;12:4539–50. https://doi.org/10.1021/ACSSUSCHEMENG.3C07731/SUPPL_FILE/SC3C07731_SI_001.PDF.
- [75] Kang S, Li X, Fan J, Chang J. Characterization of hydrochars produced by hydrothermal carbonization of lignin, cellulose, d-xylose, and wood meal. *Ind Eng Chem Res* 2012;51:9023–31. <https://doi.org/10.1021/ie300565d>.
- [76] Cai H, Lin X, Tian L, Luo X. One-step hydrothermal synthesis of carbonaceous spheres from glucose with an aluminum chloride catalyst and its adsorption characteristic for uranium(VI). *Ind Eng Chem Res* 2016;55:9648–56. <https://doi.org/10.1021/ACS.IECR.6B02540>.
- [77] Rodriguez Correa C, Hehr T, Voglhuber-Slavinsky A, Rauscher Y, Kruse A. Pyrolysis vs. hydrothermal carbonization: understanding the effect of biomass structural components and inorganic compounds on the char properties. *J Anal Appl Pyrolysis* 2019;140:137–47. <https://doi.org/10.1016/j.jaap.2019.03.007>.
- [78] Li H, Shi F, An Q, Zhai S, Wang K, Tong Y. Three-dimensional hierarchical porous carbon derived from lignin for supercapacitors: insight into the hydrothermal carbonization and activation. *Int J Biol Macromol* 2021;166:923–33. <https://doi.org/10.1016/j.ijbiomac.2020.10.249>.
- [79] E.L. Akpan S.O. *Adoesun Sustainable Lignin for Carbon Fibers: Principles, Techniques, and Applications* 2019 Springer International Publishing 10.1007/978-3-030-18792-7.
- [80] Mattsson C, Andersson SI, Belkheiri T, Åmand LE, Olausson L, Vamling L, et al. Using 2D NMR to characterize the structure of the low and high molecular weight fractions of bio-oil obtained from LignoBoost™ kraft lignin depolymerized in subcritical water. *Biomass Bioenergy* 2016;95:364–77. <https://doi.org/10.1016/j.biombioe.2016.09.004>.
- [81] Kang S, Li X, Fan J, Chang J. Hydrothermal conversion of lignin: a review. *Renew Sustain Energy Rev* 2013;27:546–58. <https://doi.org/10.1016/j.rser.2013.07.013>.
- [82] Ruan X, Liu Y, Wang G, Frost RL, Qian G, Tsang DCW. Transformation of functional groups and environmentally persistent free radicals in hydrothermal carbonisation of lignin. *Bioresour Technol* 2018;270:223–9. <https://doi.org/10.1016/j.biortech.2018.09.027>.
- [83] Kim D, Cheon J, Kim J, Hwang D, Hong I, Kwon OH, et al. Extraction and characterization of lignin from black liquor and preparation of biomass-based activated carbon therefrom. *Carbon Letters* 2017;22:81–8. <https://doi.org/10.5714/CL.2017.22.081>.
- [84] Mendoza Martinez CL, Alves Rocha EP, Oliveira Carneiro A de C, Borges Gomes FJ, Ribas Batalha LA, Vakkilainen E, et al. Characterization of residual biomasses from the coffee production chain and assessment the potential for energy purposes. *Biomass Bioenergy* 2019;120:68–76. Doi: 10.1016/j.biombioe.2018.11.003.
- [85] Svensson S. Minimizing the sulphur content in Kraft lignin. Degree Project, ECTS 300 2008.
- [86] Wielgosiński G, Lechtańska P, Namiecińska O. Emission of some pollutants from biomass combustion in comparison to hard coal combustion. *J Energy Inst* 2017; 90:787–96. <https://doi.org/10.1016/j.joei.2016.06.005>.
- [87] Energy research Centre of the Netherlands (ECN). Database for the physicochemical composition of (treated) lignocellulosic biomass, micro- and macroalgae, various feedstocks for biogas production and biochar n.d.
- [88] Hoekman SK, Broch A, Robbins C. Hydrothermal carbonization (HTC) of lignocellulosic biomass. *Energy Fuel* 2011. <https://doi.org/10.1021/ef101745n>.
- [89] Guo S, Dong X, Liu K, Yu H, Zhu C. Chemical, energetic, and structural characteristics of hydrothermal carbonization solid products for lawn grass. *BioResources* 2015;10:4613–25. <https://doi.org/10.15376/biores.10.3.4613-4625>.
- [90] Bevan E, Fu J, Luberti M, Zheng Y. Challenges and opportunities of hydrothermal carbonisation in the UK; case study in Chirnside. *RSC Adv* 2021;11:34870–97. <https://doi.org/10.1039/D1RA06736B>.
- [91] Dominik W, Pablo A, Sonja H, Fernando C, Luca F, Andrea K. Process Water Recirculation During Hydrothermal Carbonization as a Promising Process Step Towards the Production of Nitrogen-Doped Carbonaceous Materials. *Waste and Biomass Valorization* 2021 13:4 2021;13:2349–73. Doi: 10.1007/S12649-021-01603-X.
- [92] Smoliński A, Howaniec N, Stańczyk K. A comparative experimental study of biomass, lignite and hard coal steam gasification. *Renew Energy* 2011;36: 1836–42. <https://doi.org/10.1016/j.renene.2010.12.004>.
- [93] Li X, Yang C, Liu M, Bai J, Li W. Influence of different biomass ash additive on anthracite pyrolysis process and char gasification reactivity. *Int J Coal Sci Technol* 2020;7:464–75. <https://doi.org/10.1007/S40789-020-00349-6/FIGURES/7>.
- [94] U.N.E.P. Standardized Toolkit for Identification and Quantification of Dioxin and Furan Releases 2003 Geneva, Switzerland.
- [95] de Oliveira Maia BG, de Oliveira APN, de Oliveira TMN, Marangoni C, Souza O, Sellin N. Characterization and production of banana crop and rice processing waste briquettes. *Environ Prog Sustain Energy* 2018;37:1266–73. <https://doi.org/10.1002/EP.12798>.
- [96] Nunes RS, Tudino TC, Vieira LM, Mandelli D, Carvalho WA. Rational production of highly acidic sulfonated carbons from kraft lignins employing a fractionation process combined with acid-assisted hydrothermal carbonization. *Bioresour Technol* 2020;303:122882. <https://doi.org/10.1016/j.biortech.2020.122882>.
- [97] Musa U, Castro-Díaz M, Uguna CN, Snape CE. Effect of process variables on producing biochars by hydrothermal carbonisation of pine Kraft lignin at low temperatures. *Fuel* 2022;325:124784. <https://doi.org/10.1016/j.fuel.2022.124784>.
- [98] Daskin M, Erdoğan A, Güleç F, Okolie JA. Generalizability of empirical correlations for predicting higher heating values of biomass. *Energy Sources Part A* 2024;46:5434–50. <https://doi.org/10.1080/15567036.2024.2332472>.
- [99] Ischia G, Goldfarb JL, Miotello A, Fiori L. Green solvents to enhance hydrochar quality and clarify effects of secondary char. *Bioresour Technol* 2023;388: 129724. <https://doi.org/10.1016/j.biortech.2023.129724>.
- [100] Gao Y, Wang X, Wang J, Li X, Cheng J, Yang H, et al. Effect of residence time on chemical and structural properties of hydrochar obtained by hydrothermal carbonization of water hyacinth. *Energy* 2013;58:376–83. <https://doi.org/10.1016/j.energy.2013.06.023>.
- [101] Nicolae SA, Au H, Modugno P, Luo H, Szego AE, Qiao M, et al. Recent advances in hydrothermal carbonisation: from tailored carbon materials and biochemicals to applications and bioenergy. *Green Chem* 2020;22:4747–800. <https://doi.org/10.1039/D0GC00998A>.
- [102] Uddin MH, Reza MT, Lynam JG, Coronella CJ. Effects of water recycling in hydrothermal carbonization of loblolly pine. *Environ Prog Sustain Energy* 2014; 33:1309–15. <https://doi.org/10.1002/EP.11899>.
- [103] Arauzo PJ, Olszewski MP, Wang X, Pfersich J, Sebastian V, Manyá J, et al. Assessment of the effects of process water recirculation on the surface chemistry and morphology of hydrochar. *Renew Energy* 2020;155:1173–80. <https://doi.org/10.1016/j.renene.2020.04.050>.
- [104] Shrestha B, Le Brech Y, Ghislain T, Leclerc S, Carré V, Aubriet F, et al. A multitechnique characterization of lignin softening and pyrolysis. *ACS Sustain Chem Eng* 2017;5:6940–9. [10.1021/ACSSUSCHEMENG.7B01130/SUPPL_FILE/SC7B01130_SI_001.PDF](https://doi.org/10.1021/ACSSUSCHEMENG.7B01130/SUPPL_FILE/SC7B01130_SI_001.PDF).
- [105] Amit TA, Roy R, Rainie DE. Thermal and structural characterization of two commercially available technical lignins for potential depolymerization via hydrothermal liquefaction. *Current Res Green Sustain Chem* 2021;4:100106. <https://doi.org/10.1016/J.CRGSC.2021.100106>.
- [106] Lotfi S, Mollaabbasi R, Patience GS. Kinetics of softwood kraft lignin inert and oxidative thermolysis. *Biomass Bioenergy* 2018;109:239–48. <https://doi.org/10.1016/J.BIOMBIOE.2017.11.011>.
- [107] Li J, Bai X, Fang Y, Chen Y, Wang X, Chen H, et al. Comprehensive mechanism of initial stage for lignin pyrolysis. *Combust Flame* 2020;215:1–9. <https://doi.org/10.1016/J.COMBUSTFLAME.2020.01.016>.
- [108] Wądrzyk M, Janus R, Lewandowski M, Magdziar A. On mechanism of lignin decomposition – Investigation using microscale techniques: Py-GC-MS, Py-FT-IR and TGA *Renew Energy* 2021;177:942–52. <https://doi.org/10.1016/J.RENENE.2021.06.006>.
- [109] Brebu M, Tamminen T, Spiridon I. Thermal degradation of various lignins by TG-MS/FTIR and Py-GC-MS. *J Anal Appl Pyrolysis* 2013;104:531–9. <https://doi.org/10.1016/J.JAAP.2013.05.016>.
- [110] Leng E, Guo Y, Chen J, Liu S, Xue EJY. A comprehensive review on lignin pyrolysis: mechanism, modeling and the effects of inherent metals in biomass. *Fuel* 2022;309:122102. <https://doi.org/10.1016/J.FUEL.2021.122102>.
- [111] Toloue Farrokha N, Suopajarvi H, Sulasalmi P, Fabritius T. A thermogravimetric analysis of lignin char combustion. *Energy Procedia* 2019;158:1241–8. <https://doi.org/10.1016/J.EGYPRO.2019.01.413>.

- [112] Chen C, Liang W, Fan F, Wang C. The Effect of Temperature on the Properties of Hydrochars Obtained by Hydrothermal Carbonization of Waste *Camellia oleifera* Shells 2021. Doi: 10.1021/acsomega.1c01787.
- [113] Liu X, Xie M, Hu Y, Li S, Nie S, Zhang A, et al. Facile preparation of lignin nanoparticles from waste *Camellia oleifera* shell: the solvent effect on the structural characteristic of lignin nanoparticles. *Ind Crops. Prod* 2022;183. <https://doi.org/10.1016/J.INDCROP.2022.114943>.
- [114] Tang L, Xiao J, Mao Q, Zhang Z, Yao Z, Zhu X, et al. Thermogravimetric Analysis of the Combustion Characteristics and Combustion Kinetics of Coals Subjected to Different Chemical Demineralization Processes 2022;7:13998–4008. Doi: 10.1021/acsomega.2c00522.
- [115] Niu Y, Shaddix CR. A sophisticated model to predict ash inhibition during combustion of pulverized char particles. *Proc Combust Inst* 2015;35:561–9. <https://doi.org/10.1016/J.PROCLI.2014.05.077>.
- [116] Qadi N, Takeno K, Mosqueda A, Kobayashi M, Motoyama Y, Yoshikawa K. Effect of Hydrothermal Carbonization Conditions on the Physicochemical Properties and Gasification Reactivity of Energy Grass 2019. Doi: 10.1021/acs.energyfuels.9b00994.
- [117] Li Z, Guo T, Chen Y, - al, Liu P, Ma HW, et al. Thermogravimetric analysis of combustion characteristics of coal gangue and petroleum coke mixture. *J Phys Conf Ser* 2019;1324:012077. Doi: 10.1088/1742-6596/1324/1/012077.
- [118] Wnorowska J, Ciukaj S, Kalisz S. Thermogravimetric Analysis of Solid Biofuels with Additive under Air Atmosphere. *Energies* 2021, Vol 14, Page 2257 2021;14: 2257. Doi: 10.3390/EN14082257.
- [119] Xinjie L, Singh S, Yang H, Wu C, Zhang S. A thermogravimetric assessment of the tri-combustion process for coal, biomass and polyethylene. *Fuel* 2021;287: 119355. <https://doi.org/10.1016/J.FUEL.2020.119355>.
- [120] Wang J-H, Chang L-P, Li F, Xie & K-C, Xie K-C. A Study on the Combustion Properties of Western Chinese Coals. *Energy Sources* 2010;32:1040–51. Doi: 10.1080/15567030802606327.
- [121] Zhang L, Chen K, Peng L. Comparative research about wheat straw lignin from the black liquor after soda-oxygen and soda-AQ pulping: structural changes and pyrolysis behavior. *Energy Fuel* 2017;31:10916–23. <https://doi.org/10.1021/ACS.ENERGYFUELS.7B01786>.
- [122] Lucejko JJ, Tamburini D, Modugno F, Ribechini E, Colombini MP. Analytical pyrolysis and mass spectrometry to characterise lignin in archaeological wood. *Applied Sciences (Switzerland)* 2021;11:1–25. <https://doi.org/10.3390/app11010240>.
- [123] van der Hage ERE, Mulder MM, Boon JJ. Structural characterization of lignin polymers by temperature-resolved in-source pyrolysis-mass spectrometry and Curie-point pyrolysis-gas chromatography/mass spectrometry. *J Anal Appl Pyrolysis* 1993;25:149–83. [https://doi.org/10.1016/0165-2370\(93\)80038-2](https://doi.org/10.1016/0165-2370(93)80038-2).
- [124] Caboni P, Sarais G, Cabras M, Angioni A. Determination of 4-ethylphenol and 4-ethylguaiacol in wines by LC-MS-MS and HPLC-DAD-fluorescence. *J Agric Food Chem* 2007;55:7288–93. <https://doi.org/10.1021/JF071156M>.
- [125] Takada D, Ehara K, Saka S. Gas chromatographic and mass spectrometric (GC-MS) analysis of lignin-derived products from *Cryptomeria japonica* treated in supercritical water. *J Wood Sci* 2004;50:253–9. <https://doi.org/10.1007/s10086-003-0562-6>.
- [126] Tanruean K. Bioconversion of ferulic acid into high value metabolites by white rot fungi isolated from fruiting-body of the polypore mushroom. *J Med Bioeng* 2013; 2:168–72. <https://doi.org/10.12720/JOMB.2.3.168-172>.
- [127] Wheeler TF, Heim JR, Latorre MR, Janes AB. Mass spectral characterization of p-*nonylphenol* isomers using high-resolution capillary GC-MS. *J Chromatogr Sci* 1997;35.
- [128] Pan Z, Puente-Urbina A, Bodi A, van Bokhoven JA, Hemberger P. Isomer-dependent catalytic pyrolysis mechanism of the lignin model compounds catechol, resorcinol and hydroquinone. *Chem Sci* 2021;12:3161. <https://doi.org/10.1039/D1SC00654A>.
- [129] Rao H, Li P, Wu H, Liu C, Peng W, Su W. Simultaneous determination of six compounds in destructive distillation extracts of hawthorn seed by GC-MS and evaluation of their antimicrobial activity. *Molecules* 2019;24. Doi: 10.3390/MOLECULES24234328.
- [130] Guo G, Zhang K, Liu C, Xie S, Li X, Li B, et al. Comparative investigation on thermal decomposition of powdered and pelletized biomasses: thermal conversion characteristics and apparent kinetics. *Bioresour Technol* 2020;301: 122732. <https://doi.org/10.1016/J.BIORTECH.2020.122732>.
- [131] Soongpravit K, Sricharoenchaikul V, Atong D. Phenol-derived products from fast pyrolysis of organosolv lignin. *Energy Rep* 2020;6:151–67. <https://doi.org/10.1016/J.EGYR.2020.08.040>.
- [132] Supriyanto UDO, Ylittervo P, Dou J, Sipponen MH, Richards T. Identifying the primary reactions and products of fast pyrolysis of alkali lignin. *J Anal Appl Pyrolysis* 2020;151:104917. <https://doi.org/10.1016/J.JAAP.2020.104917>.
- [133] Zhao Y, Deng L, Liao B, Fu Y, Guo QX. Aromatics production via catalytic pyrolysis of pyrolytic lignins from bio-oil. *Energy Fuel* 2010;24:5735–40. 10.1021/EF100896Q/SUPPL_FILE/EF100896Q_SI_001.PDF.
- [134] Pola L, Collado S, Oulego P, Díaz M. Hydrothermal processing of Kraft lignin for carboxylic acid production. *J Environ Chem Eng* 2019;7. <https://doi.org/10.1016/j.jece.2019.103472>.
- [135] Sermyagina E, Mendoza Martinez CL, Nikku M, Vakkilainen E. Spent coffee grounds and tea leaf residues: characterization, evaluation of thermal reactivity and recovery of high-value compounds. *Biomass Bioenergy* 2021;150:106141. <https://doi.org/10.1016/j.biombioe.2021.106141>.
- [136] Ajao O, Benali M, Faye A, Li H, Maillard D, Ton-That MT. Multi-product biorefinery system for wood-barks valorization into tannins extracts, lignin-based polyurethane foam and cellulose-based composites: techno-economic evaluation. *Ind Crops Prod* 2021;167:113435. <https://doi.org/10.1016/J.INDCROP.2021.113435>.
- [137] Axegård P, STFI-Packforsk. The kraft pulp mill as a biorefinery. In: Proceedings of the 3rd ICEP: International Colloquium on Eucalyptus Pulp, Belo Horizonte, Brazil: 2007, p. 1–6.
- [138] Tomani P, Axegard P, Berglin N, Nordgren D, Berghel T. LignoBoost Kraft Lignin-A New Renewable Fuel and a Valuable Fuel Additive. International Bioenergy & Bioproducts Conference, Atlanta GA, USA: 2021.
- [139] Mazar A, Paleologou M. Comparison of the effects of three drying methods on lignin properties. *Int J Biol Macromol* 2024;258:128974. <https://doi.org/10.1016/J.IJBIOMAC.2023.128974>.
- [140] Saari J, Mendoza-Martinez C, Kuparinen K, Lipiäinen S, Hamaguchi M, Cardoso M, et al. Techno-economic analysis of hydrothermal carbonization of pulp mill biosludge. *Tappi J* 2023;3:206–16. <https://doi.org/10.32964/TJ22.3.206>.